Service Life Assessment of Internal Replacement Pipe: External Load Testing of Generic Epoxy Material

Final Testing Report

Prepared for:

DOE/ARPA-E REPAIR

Prepared by:

REPAIR Testing & Analysis Team

Center for Infrastructure, Energy, and Space Testing
University of Colorado Boulder

Molly Sickler
Sina Senji
Cory Ihnotic
Brad P. Wham

May 2025

Table of Contents

Table of Figures

Table of Tables

Acknowledgements

The authors thank DOE/ARPA-E for financially supporting this research and for guiding our progress throughout its execution, in particularly, we thank Dr. Jack Lewnard, Dr. Sade Ruffin, and Matthew Hackworth for their leadership of the Rapid Encapsulation of Pipelines Avoiding Intensive Replacement (REPAIR) program. The team extends its gratitude to the Technical & Testing Specifications Pannel (TTSP), who provided valuable practical feedback and industry guidance through the project. We thank the staff and students at the University of Colorado at Boulder, University of Southern Queensland, and Cornell University for their many contributions to the REPAIR project as well as the work presented herein. We appreciate the manufacturer's donation of test specimens and support through technical discussions.

The information, data, or work presented herein was funded in part by the Advanced Research Projects Agency-Energy (ARPA-E), US Department of Energy under Award No. DE-AR0001327. The views and opinions of authors expressed herein do not necessarily state or reflect those of the United States Government or any agency thereof.

1 Introduction & Background

Compared to the open trench method, trenchless technology (TT) for water, wastewater, oil and gas pipelines are used increasingly to replace incident-prone legacy pipes. TT results in less environmental damage, the minimization of excavation activities, and lower costs compared to open cut methods (Allouche et al., 2014; Lu et al., 2020; Najafi, 2005; Vladeanu & Matthews, 2018). There has been much effort to develop internal replacement pipe (IRP) technologies as well as the formal standards and documents concerning these technologies (Pipeline Infrastructure Committee 2021; ASME PCC-2 Article 403 2018; ASTM F1216 2016a; ASTM F3182 2016b; ASTM F1743 2017; ASTM D5813 2018; ASTM F2207 2019a; AWWA Committee 2019). Nevertheless, there are some outstanding questions about IRP technologies, including long-term suitability and performance, practical considerations for external loads, and the role of adhesion in the structural capacity and response. Legacy host pipes undergo various failure modes depending on the type of loading. Moreover, studies are lacking for the long-term response of deteriorated host pipes to external loads (Dixon et al., 2023b; Fu et al., 2020).

This report addresses external loads affecting IRP technologies. It presents lab-based methods for evaluating IRP over a 50-year service-life with repaired pipe specimens. The specimens studied featured a generic structural epoxy repair material, provided by an ARPA-E Awardee Team, which is considered a “developer” material that is currently under development. The intended external loads are traffic loading, ground movement due to adjacent excavations, and thermally-induced axial deformation of the repaired system. This report is a logical extension of earlier work performed at Cornell University (Jeon et al., 2004; Stewart et al., 2015), which developed an evaluation framework for cured-in-place liners (CIPLs) under external loads. The framework developed at Cornell University assumed negligible mechanical contribution (stiffness) of liner to the pipeline response, which was a conservative and appropriate assumption considering the type of materials that were evaluated by researchers at the time. The current team has altered this aspect in their framework, now accounting for the stiffness of a repair pipe in the estimation of field deformations. The numerical and analytical methods to estimate field deformations of the generic epoxy IRP are outlined briefly in this report. Detailed test methods and major results are presented. Important observations and aspects of the testing are discussed.

2 Methodology of Mechanical Aging Tests

The following section describes the test methodology to simulate major aspects of the external loading of an internal REPAIR pipe over a 50-year service-life in the field. The approach applies laboratory loading to mimic deformations applied by traffic loading, adjacent excavations, and seasonal temperature fluctuation.

2.1 Lateral Loading

2.1.1 Model Description

The imposed deformations associated with transverse testing are based on approaches defined by Klingaman et al., (2025). In summary, a "beam-on-springs" finite element (FE) model was developed in OpenSees for a buried cast iron pipeline subjected to traffic loading and soil displacements representative of adjacent excavation activity. The pipeline elements were represented by 3 in. (75 mm) long, 1D Euler-Bernoulli beam elements. A circumferential gap opening (also referred to as crack) was modeled by removing host pipe elements. For the cases in which an IRP repair was combined with the host pipe, the missing element or gap was replaced with a beam element with properties of the IRP material and length equal to the width of the gap opening. CI joints were modeled using rotational, shear, and axial springs. Soil was represented using soil springs with a hyperbolic force-displacement.

2.1.2 Traffic Loading

As described in detail by Klingaman et al., (2022), traffic loading was derived from an HS-20 design truck and was conservatively increased to 30 kips (130 kN). The resulting traffic load was assumed to be applied at the ground surface according to the Boussinesq stress distribution for a point load on a semi-infinite elastic medium. The stress calculated at a depth of 30 in. (762 mm) was multiplied by the vertically projected area of the pipe (diameter times element size) and discreetly applied to each pipeline node in the FE model (Figure 1). Resulting pipe deformations (e.g., relative rotations) were recorded so that they could be applied in the lab.

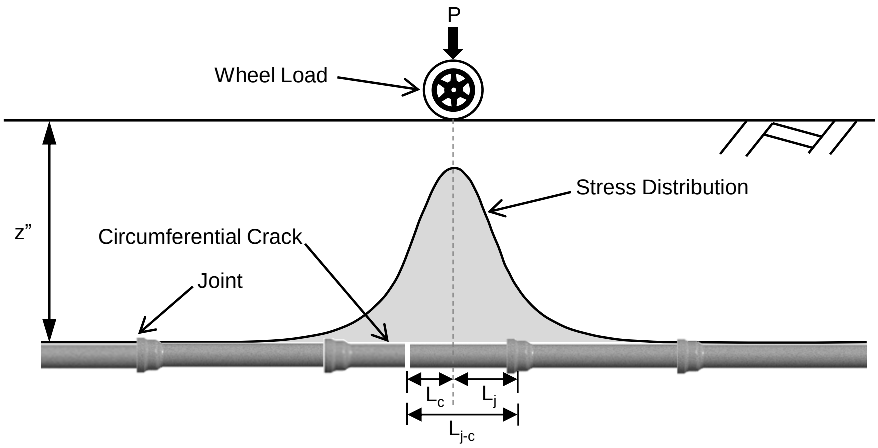

Figure 1. Schematic of traffic loading scenario

2.1.3 Adjacent Excavation (AE)

As described by Klingaman et al., (2025), soil displacement profiles were developed using a functional form proposed by Roboski & Finno (2006), which requires 3 inputs: excavation depth, H_e, maximum soil displacement, d_{max}, and the length over which d_{max} is developed, L. The adjacent excavation (AE) depth was assumed to be 20 ft. (6 m), various values of d_{max} were considered, ranging from 2.5-10 in. (63.5-254 mm), and L was assumed to be 50 ft. (15.2 m) (Figure 2). The soil displacements were applied to each soil node in the FE model and resulting rotations were recorded so that they could be applied in the lab. During this study, the smaller and larger parallel (adjacent) excavation events, typically referred to as PE1 and PE2 for each specimen, were associated with d_{max} of 2.5 in. (63.5 mm) and 5 in. (127 mm), respectively.

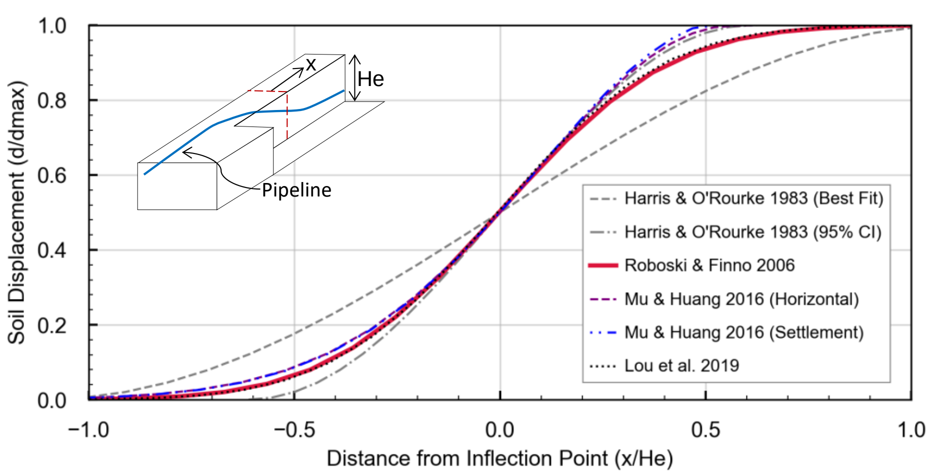

Figure 2. Soil displacement profiles parallel (adjacent) to an excavation from previous studies

2.2 Thermal Loading

Temperature fluctuations in soil will give rise to axial deformation and/or induced axial load in repaired systems from thermal expansion. Previous work used 40°F (22.2°C) as the annual soil temperature variation in New York state (Stewart et al., 2015). This work includes temperature variations of 40°F (22.2°C) and 50°F (27.8°C) and considers granular soil as the backfill material in contact with the host pipe. Additionally, this work considers the stress-free state of the system to be the highest temperature (T_{max}), such that all temperature variation is negative. To understand the problem, a mechanics based analytical approach has been developed as shown in Figure 3 (Dixon et al., 2023a).

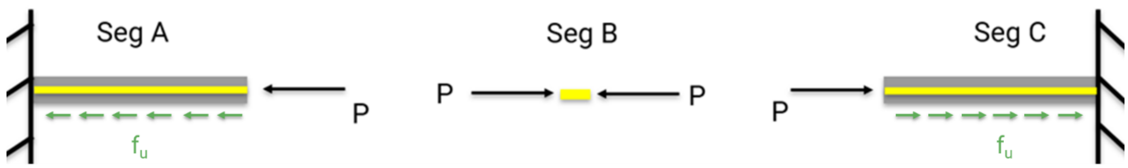

Figure 3. Fully bonded approach schematic with friction from pipe-soil interaction

The specimen is divided into three regions/segments: Segment A refers to combined host and REPAIR section, and Segment B refers to the exposed REPAIR pipe region (Segment C would refer to the other combined host and REPAIR section but symmetry allows the use of only Segment A and B). The host and repair pipe are treated as fully bonded in Segment A. Simple analytical expressions for the fully unbonded case are straightforward, and it is noted as the gap width (length of Segment B) approaches the system length, induced loads calculated with a fully-bonded assumption approach those for the unbonded case. Furthermore, even in "unbonded" systems some level of intimate mechanical contact is necessary for successful installation, and so the initial assumption will be fully bonded (if results from initial assessments with small levels of axial displacement demonstrate a fully unbonded system then the unbonded approach will be used). In this approach Segment A acts as a single unit, i.e., combined section properties and thermo-mechanical response with no differential displacement between the repair and host within the segment. Soil friction, f_u, is accounted for in the approach. Compatibility between the segments is used to solve for the induced load, which then can be used to determine the elongation of Segment B, i.e., the crack/gap opening displacement (COD). The forementioned assumptions are intended to produce the largest expected deformation at the crack, and therefore establish a conservative estimate of thermally induced displacement.

This approach is leveraged with previous work, finite element models, and knowledge about the generic epoxy liner to obtain target displacements for axial loading (e.g., Ahmadi et al., 2024) that are conservative in magnitude (i.e., displacements greater than those that more detailed methods) and hence a safety factor on target displacements was taken as 1.0.

3 Test Specimens and Material

Specimens consisted of 12 in. (305 mm) nominal diameter steel host pipes repaired with a generic epoxy material. Straight specimen consisted of two segments of host pipe, arranged such that, when repaired, full circumferential (ring) gaps of exposed liner are present near the center of the specimen. This condition is intended to represent a worst-case scenario which the IRP would need to accommodate during its service life. The nominal gap widths ranged from 0.5 in. (12.7 mm) to 6 in. (152.4 mm). The former dimension reflects a partially displaced (pulled-out) joint in a legacy cast-iron gas distribution system, which is still functional (determined from utility input), and the latter dimension corresponds to a region of extreme deterioration of host pipe post-repair. These circumferential cracks are fairly severe, requiring the load to be carried entirely by the repair pipe over a section while simultaneously capturing interactions between host and repair pipe that potentially could give rise to stress concentrations and failures, which would not be observed in the host pipe alone.

This generic epoxy was deposited into the pipe by spraying the fluid material through a high-pressure nozzle on to the interior pipe surface. The components of the epoxy are mixed during the deposition process such that the material rapidly cures in place.

Full-scale test specimens and flat plate samples were prepared by the manufacturer at their facilities. Host pipes were shipped in specially designed crates to the manufacturer, and the specimens were prepared following expected installation procedures and then shipped back to the respective testing laboratories. The internal surfaces of the steel host pipe segments were unprotected. No treatment was applied to them prior to lining.

Straight specimen repairs were performed with the manufacturer's robot, still in development, shown in Figure 4. The robot was capable of lining the full length of the specimens with predictable thickness throughout. The non-uniform specimens were lined manually, which resulted in greater variation in thickness along the bends of the specimens.

Figure 4. Repair robot under development

3.1 <u>Material Characterization</u>

Tensile coupon tests were performed at CIEST and GTI Energy. The purpose of these tests is to determine the tensile properties of the generic epoxy. A total of twelve specimens were prepared from flat panels prepared by the manufacturer. All tensile coupons were subjected to testing until capacity. Their corresponding load, deflection, and strain values were recorded to establish the material properties.

The tensile testing of the epoxy material was carried out in accordance with ASTM D638 – 2014, utilizing specimens provided to CUB. The tensile test setup is depicted in Figure 5. The specimens were subjected to a tensile load at a rate of 1.3 mm/min using a 11 kip Instron UTM. An extensometer was affixed to the middle of the specimen. From this test, the maximum load, modulus of elasticity, ultimate tensile strength and failure strain are reported.

Figure 5. Test set-up for tensile test

3.1.1 Coupon Test Results

Figure 6 shows the tensile test stress vs. strain behavior of the epoxy tensile coupons, respectively. Table 1 provides a summary of the results, including ultimate tensile strength, and modulus of elasticity. The modulus of elasticity is determined by taking the average of the initial stiffnesses of all tested coupons. The average Poisson's ratio, 0.318, was determined from two coupon samples that included bi-axial strain gauges.

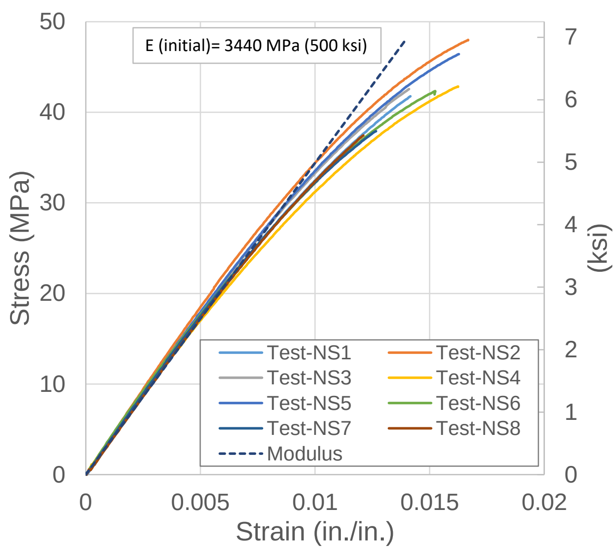

Figure 6. Test results for tensile coupon stress-strain behavior

Table 1. Tensile coupon test results

Sample ID	Elastic of Modulus		Ultimate stress	
	(GPa)	(ksi)	(MPa)	(ksi)
NS1	3.41	494	41.8	6.06
NS2	3.61	524	48.0	6.96
NS3	3.49	505	42.6	6.17
NS4	3.30	479	42.9	6.21
NS5	3.51	509	46.4	6.73
NS6	3.42	496	42.3	6.14
NS7	3.41	494	37.9	5.50
NS8	3.37	489	37.4	5.43
Average	**3.44**	**499**	**42.4**	**6.15**
STDEV	94	14	3.6	0.53

The generic epoxy tensile coupons exhibited initial elastic behavior followed by fracture. Figure 7 shows a photo of dog bone specimens before testing and Figure 8 provides a typical example of a failed specimen.

Table 2. Tensile coupon result summary

Test	Ultimate Strength		Modulus of Elasticity		Failure Strain	
	(MPa)	(ksi)	(GPa)	(ksi)	(mm/mm)	(%)
Tensile	42.4	6.15	3.44	499	0.015	1.5

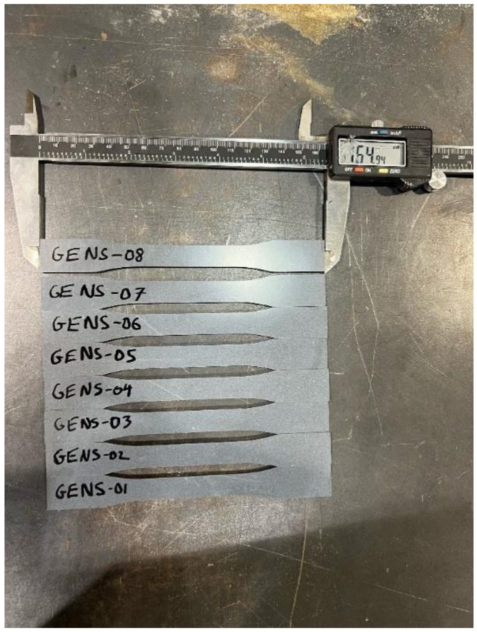

Figure 7. Photo of coupon specimens, "GE" stands for generic epoxy

Figure 8. Tensile coupons test setup post-test

3.2 Test Specimen Design

Test specimens include both traditional straight pipe assemblies as well as bent or offset specimens that are constructed with a series of angled couplings resulting in a geometrically non-uniform assembly.

Traditional straight pipe assemblies are prepared using two 12 in. (305 mm) diameter, 60 in. (1520 mm) long host pipe segments, shown in Figure 9. The pipe segments are set up such that an initial crack opening is present. The repair material is then applied inside the host pipe, across the initial crack opening, such that the specimen is joined to create a single testing specimen. One side of the specimen includes pipe defects along the host pipe, including varying sized holes and "existing" service connections.

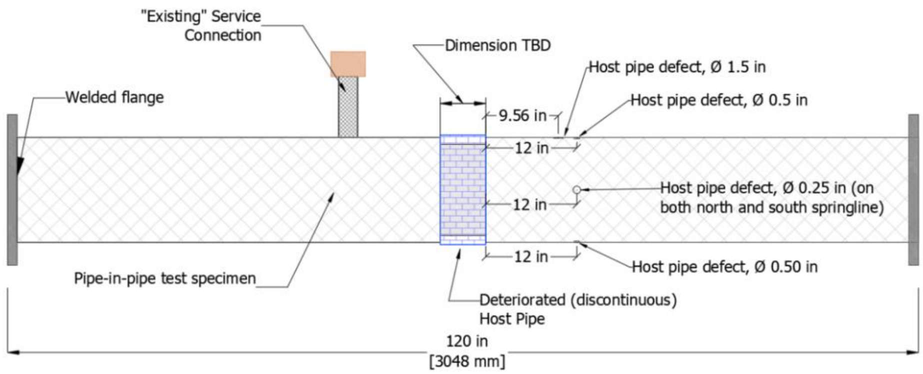

Figure 9. Dimensioned drawings of uniform specimens

The non-uniform test specimens are constructed using several straight pipe segments joined together with two 22° flanged couplings and one 45° flanged coupling, shown in Figure 10. Two initial gap openings of 0.5 in. (12.7 mm) are included on either side of the 45° flanged coupling, and the repair material is then applied inside the host pipe, across the crack openings, such that the specimen is joined to create a single testing specimen.

(a)

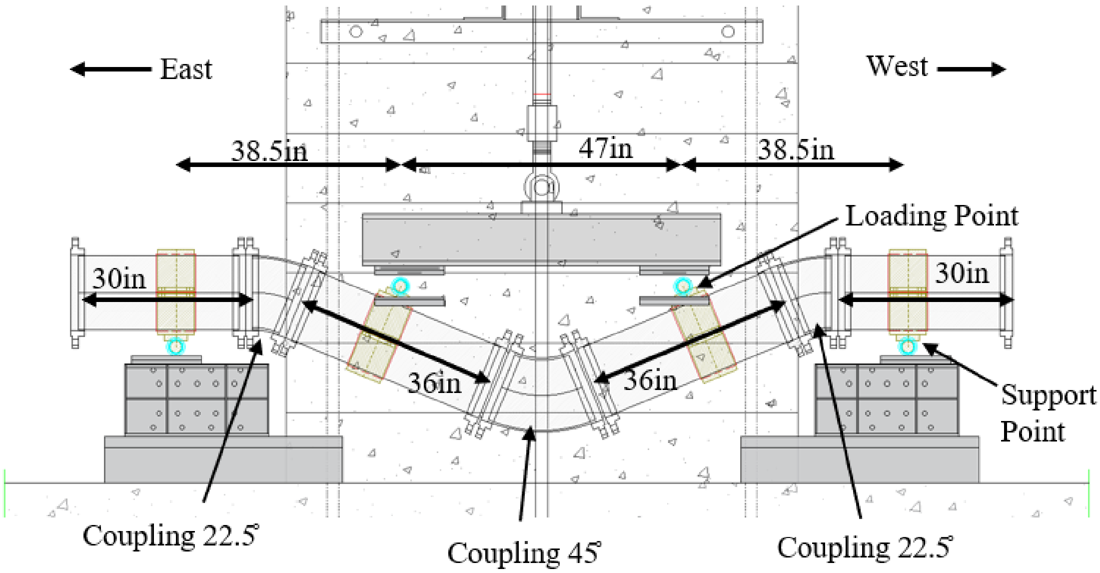

(b)

Figure 10. Dimensioned drawings of non-uniform specimens

4 Experimental Methods

This section describes the procedures performed on the test specimens. The section is divided into bending and axial sections, and are further broken down to detail specific specimen variations. All specimens are tested using the Structural Testing System (STS) at CIEST. General methods are similar among the specimens, but differences in exact instrumentation and methods warrant such a breakdown. The four specimens tested for this project are as follows: GE01 - steel host pipe with a nominal gap width of 6.0 in. (152 mm); GE02 - steel host pipe with a nominal gap width of 0.5 in. (12.7 mm); GE_B01 and GE_B02 – non-uniform steel host pipe with two nominal gap widths of 0.5 in. (12.7 mm), where GE refers to generic epoxy. Specimen details are given in Table 3.

Table 3. Generic epoxy test specimen overview

Specimen Label*	Host Pipe Material: OD (in. [mm])*	Nominal Crack Width (in. [mm])	Specimen Length (in. [m])	Dates under Test
GE01	Steel: 12.75 [324]	0.5 [12.7]	127 [3.23]	9/5/2024-9/25/2024
GE02	Steel: 12.75 [324]	6.0 [152.4]	133 [3.38]	10/22/2024-10/24/2024
GE_B01	Steel: 12.75 [324]	0.5 [12.7] *2	160 [4.06]	12/12/2024- 1/17/2025
GE_B02	Steel: 12.75 [324]	0.5 [12.7] *2	160 [4.06]	2/3/2025-2/19/2025

* GE nomenclature refers to generic epoxy IRP material

4.1 Transverse Loading

All specimens are first tested in a four-point bending configuration with a 22-kip (100 kN) actuator at CU Boulder. Testing saddles at loading and support points are used to distribute applied loads, minimizing localized stress concentrations. Strain gauges (SGs), string pots (SPs), and linear variable differential transducers (LVDTs) are applied to all specimens to record strains and displacement at various points of interest. Figure 11 shows a schematic of loading applied for transverse testing. Figure 12 provides a schematic of the test arrangement featuring the measurement devices and their respective positions for traditional test setups, while Figure 13 provides a similar schematic for the test specimens that include the angled flanged couplings. The spacing of the sensors and clamps in each schematic are listed in detail for each specimen in tables presented in the following sections.

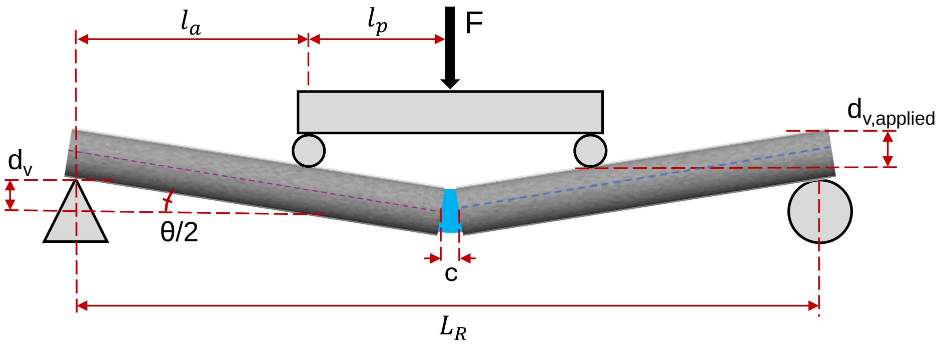

Figure 11. Schematic of 4-pt bending test and rotation angle, θt (adapted from Klingaman et al. 2022).

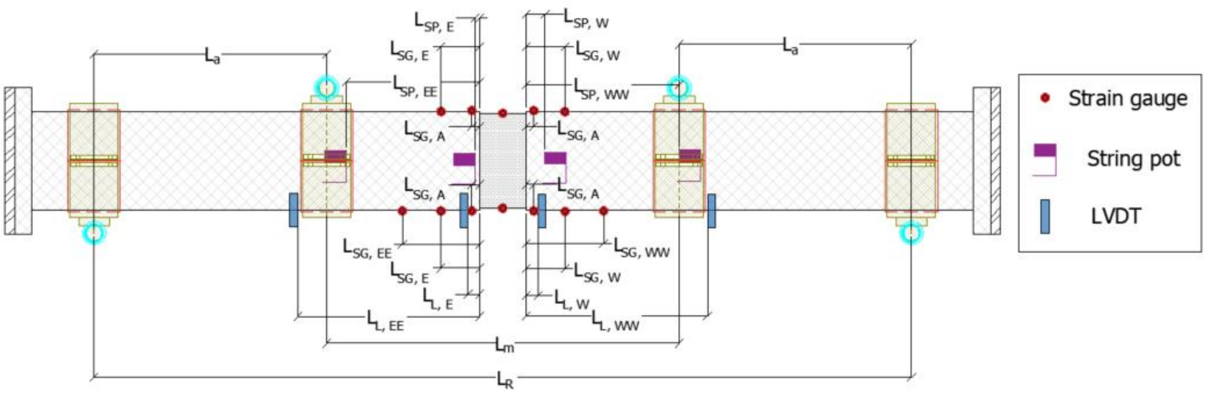

Figure 12. Test instrumentation schematic and dimension for uniform specimens

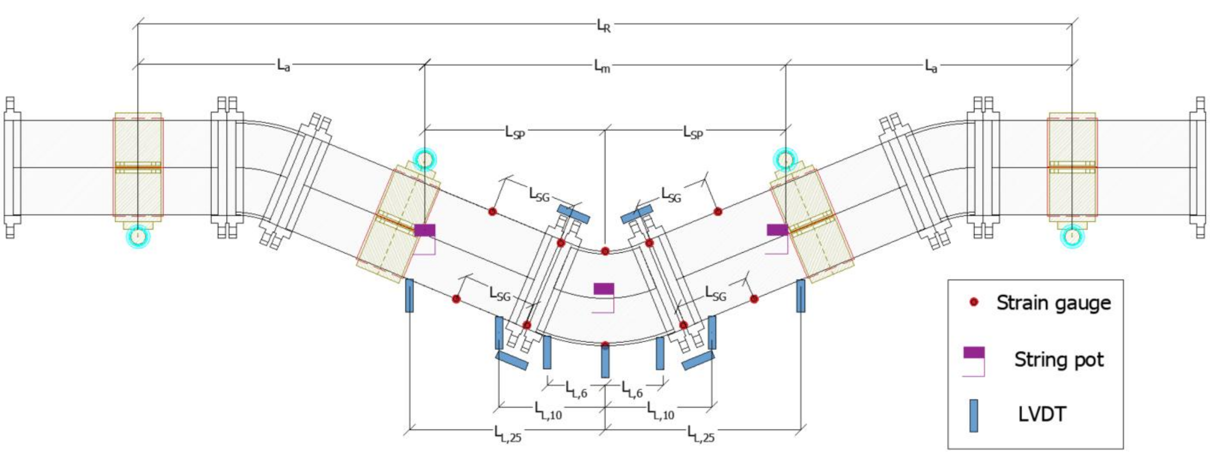

Figure 13. Test instrumentation schematic and dimensions for non-uniform specimens

The primary characteristic of four-point bending is the application of a constant moment ($M_{central}$) across the central section of the specimen that separates the two load points [i.e., 2* L_L = 40 in. (1016 mm)]. The moment increases from zero to $M_{central}$ along the specimen between the load and support points [e.g., L_s= 25 in. (625 mm)]. The moment applied to the central portion of the specimen, $M_{central}$, was calculated as

$$M_{central} = \frac{P(L_s)}{2} \tag{1}$$

in which P is the load applied by the actuator to the load beam plus the vertical force of the load beam [e.g., 0.23 kips (1.02 kN)].

Global rotation, also referred to as rotation, is reported herein to characterized specimen deformation and is taken as the relative rotation at the pipeline center between straight line projections of the pipes either side of the gap. The LVDTs between the load points (notation: E & W) were used with distance from the support points for global rotation calculations, such that:

$$\theta_t \text{ (degrees)} = 2 * tan^{-1}\left[\frac{average\left(d_{v,E}\,, d_{v,W}\right)}{(L_L + L_s - 0.5c - average(L_{L,E}\,, L_{L,W})}\right] \tag{2}$$

for which $d_{v,E}$ and $d_{v,W}$ are the relative vertical displacements between the support points and the nearest displacement device (typically LVDT) positioned on either side of the gap. The distances L_L , L_s, and c are depicted in Figure 11 and reported in subsequent sections. As shown in Figure 12, $L_{L,E}$ and $L_{L,W}$ are the LVDT distance from the gap edge and are reported for each test in the tables of subsequent sections.

All setups feature saddles fitted to the pipe and cages about saddle rollers at both the loading and support points of the specimens. The saddle and cage system allows the pipeline to return to its initial position without being lifted off its support points, thus simulating deflection in the field wherein the pipeline in soil returns to its original position after rolling traffic loads move across the pipe. For some operations, these cages are loosened, but for most testing, the cages are tightened (exceptions clearly noted). Between tests, specimens are supported by jacks to avoid specimen sag under self-weight. The crossbeam used to distribute load is also lifted away from the specimen and supported by restraining chains between each test.

Several preliminary lateral tests are performed on each specimen to check that instrumentation is functioning properly. Data recorded from these preliminary tests are also used to assess the initial lateral stiffness of the specimen. Once target rotations are established, traffic loading cycles are performed at cyclic frequencies of 1 Hz and 2 Hz, associated with sample rates of 64 Hz and 128 Hz, respectively. All traffic cycles are performed with constant pressure ranging from 10 psi to 65 psi.

Approximately 500,000 traffic loading cycles are performed on each specimen. Cycles are applied in sets to allow for setup, sensor adjustments, and ease of general lab use. To begin a new traffic cycle set, the actuator is first powered on so the restraining chains supporting the crossbeam weight can be removed. The crossbeam is then lowered to contact the specimen so that cages can be secured around the loading saddles. Once secured to the actuator, the position of the actuator is noted, and the supporting jacks are removed. Specimens are then pressurized to the desired internal pressure prior to beginning cycles. After cycles are concluded for the day, the actuator is returned to its initial position before putting the supporting jacks under the specimen. Cages are removed and the actuator is then lifted away from the pipe. This process is repeated for every test performed. Internal water pressure ranges from 10 psi (69 kPa) to 65 psi (450 kPa) over the duration of testing.

After 500,000 traffic cycles are performed, two larger lateral displacements are applied, simulating the effects of ground motions caused by adjacent excavation events. These tests are conducted with a constant internal pressure of 65 psi. The cages used to secure the specimen to the actuator are loosened prior to these tests to ensure freedom of rotation and translation for each support and loading point. Targets for each specimen are specified in the later sections. Once the first excavation event is reached, the actuator is returned to the initial test position before applying the larger of the two AE deformations.

After larger deformations are applied, the specimens are then subjected to 100,000 more traffic cycles to analyze longer term effects caused by larger deformations. These cycles are performed using the same methods previously described. Transverse loading is concluded at the end of these additional cycles. Differences between instrumentation, specimen design, and other testing variations between each specimen are outlined in the following sections.

4.1.1 GE01

The specimen for GE01 is composed of a steel host pipe with an average measured gap opening of 6.3 in. (160 mm) and rehabilitated with generic epoxy. The geometry of the specimen was set up in a 4-point bending configuration, with distances between supports and load points being 30 in. – 40 in. – 30 in. (762 mm – 1016 mm - 762 mm), centered about the crack opening.

The instrumentation used for GE01 during lateral testing is outlined in Table 4. The instrumentation consisted of strain gauges on the crown and invert over the middle 40 in. (1000 mm) (maximum moment) span in the vicinity of the crack. Linear variable differential transducers (LVDTs) and string potentiometers (SPs) were vertically arranged to measure pipe deflection at various locations on the beam. LVDTs were mounted on stands on the ground and the rods were connected to the pipes with brackets or screw sockets. SPs were mounted on the pipe, stands on the grounds, and beams extending from the strong wall (frame support). Additionally, the north facing side of the pipe over and in the vicinity of the gap was painted white and speckled black for digital image correlation (Figure 14) (see Appendix A for further discussion of DIC). Figure 12 provides a schematic of specimen measurements and instrumentation locations and Table 5 gives the values corresponding to the figure used for this specimen.

Table 4. GE01 bending instrumentation

Instrument Description	Local Instrument Name	Location	Channel No.
Strain gage, biaxial	SG5E_CA	On steel host pipe, crown, east side 5 in. from crack edge	Ch 0
Strain gage, biaxial	SG1E_CA	On steel host pipe, crown, east side 1 in. from crack edge	Ch 1
Strain gage, biaxial	SG0_CA	On liner, crown, center	Ch 2
Strain gage, biaxial	SG1W_CA	On steel host pipe, crown, west side 1 in. from crack edge	Ch. 3
Strain gage, biaxial	SG5W_CA	On steel host pipe, crown, west side 5 in. from crack edge	Ch. 4
Strain gage, biaxial	SG10E_IA	On steel host pipe, invert, east side 10 in. from crack edge	Ch. 5
Strain gage, biaxial	SG5E_IA	On steel host pipe, invert, east side 5 in. from crack edge	Ch. 6
Strain gage, biaxial	SG1E _IA	On steel host pipe, invert, east side 1 in. from crack edge	Ch. 7 .
Strain gage, biaxial	SG0_IA	On liner, invert, center	Ch. 8
Strain gage, biaxial	SG1W_IA	On steel host pipe, invert, west side 1 in. from crack edge	Ch. 9
Strain gage, biaxial	SG5W_IA	On steel host pipe, invert, west side 5 in. from crack edge	Ch. 10
Strain gage, biaxial	SG10W_IA	On steel host pipe, invert, west side 10 in. from crack edge	Ch 11
Strain gage, biaxial	SG0_CC	On liner, Crown, center	Ch 12
Strain gage, biaxial	SG0 _IC	On liner, Invert, center	Ch. 13
Strain gage, biaxial	SG1W_IC	On steel host pipe, invert, west side 1 in. from crack edge	Ch. 14

Strain gage, biaxial	SG1E_IC	On steel host pipe, invert, east side 1 in. from crack edge	Ch.15
String potentiometer, 20 in. displacement	SP WW 28-20	On west saddle (centered), south springline, 19.75 in. from crack edge	SP0
String potentiometer, 10 in. displacement	SP W 24-10	On steel host pipe, west side, south springline, 2.5 in. from crack edge	SP1
String potentiometer, 10 in. displacement	SP E 29-10	On steel host pipe, east side, south springline, 0.5 in. from crack edge	SP2
String potentiometer, 3.8 in. displacement	SP EE 21-3	On east saddle (centered), south springline, 19.75 in. from crack edge	SP3
LVDT, AC	LVDT0 1001-EE	On backet on steel, west, invert, 23 in. from crack edge	LVDT Ch. 0
LVDT, AC	LVDT1 1002-E	On backet on steel, west, invert, 1.5 in. from crack edge	LVDT Ch. 1
LVDT, AC	LVDT2 1003-W	On backet on steel, east, invert, 1.5 in. from crack edge	LVDT Ch. 2
LVDT, AC	LVDT 1004-WW	On backet on steel, east, invert, 23 in. from crack edge	LVDT Ch. 3
110-kip Load Cell	Applied Force	MTS Crosshead (Above Specimen)	
MTS Actuator Piston Position		MTS Crosshead (Above Specimen)	
150 psi Pressure Transducer	N/A	West endcap of specimen	Ch. 20

* VSP: vertical string pot, LVDT: linearly varying differential transducer, SG: foil stain gage

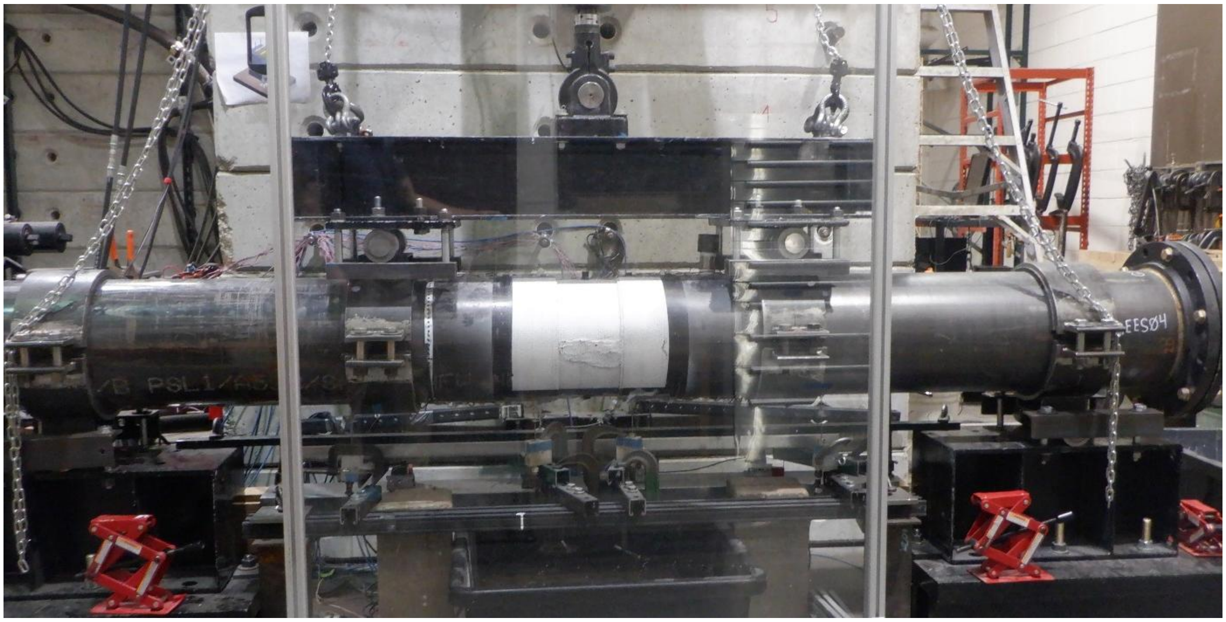

Figure 14. Image of GE01 in bending setup

Table 5. GE01 instrumentation schematic dimensions

Sensor / Measurement	Symbol	Distance
Strain Gauge (EE)	$L_{SG, EE}$	10 in
Strain Gauge (E)	$L_{SG, E}$	5 in
Strain Gauge (W)	$L_{SG, W}$	5 in
Strain Gauge (WW)	$L_{SG, WW}$	10 in
Strain Gauge (additional)	$L_{SP, A}$	1 in
String Pot (EE)	$L_{SP, EE}$	19.75 in
String Pot (E)	$L_{SP, E}$	0.5 in
String Pot (W)	$L_{SP, W}$	2.5 in
String Pot (WW)	$L_{SP, WW}$	19.75 in
LVDT (EE)	$L_{L, EE}$	23 in
LVDT (E)	$L_{L, E}$	1.5 in
LVDT (W)	$L_{L, W}$	1.5 in
LVDT (WW)	$L_{L, WW}$	23 in
Distance between reaction and applied force	L_a	30 in
Distance between reactions	L_R	100 in
Distance between applied forces	L_m	40 in

4.1.2 GE02

The specimen for GE02 composed of a steel host pipe with an average measured gap opening of 0.2 in. (5 mm) and rehabilitated with generic epoxy IRP. The geometry of the specimen was set up in a 4-point bending configuration, with distances between supports and load points being 30 in. – 40 in. – 30 in. (762 mm – 1016 mm - 762 mm), centered about the crack opening.

The instrumentation used for GE02 during lateral testing is outlined in Table 6. The instrumentation consisted of strain gauges on the crown and invert over the middle 40 in. (1000 mm) (maximum moment) span in the vicinity of the crack. Linear variable differential transducers (LVDTs) and string potentiometers (SPs) were vertically arranged to measure pipe deflection at various locations on the beam. LVDTs were mounted on stands on the ground and the rods were connected to the pipes with brackets or screw sockets. SPs were mounted on the pipe, stands on the grounds, and beams extending from the strong wall (frame support). Figure 15 shows a picture of the test setup for GE02 prior to testing. Figure 12 provides a schematic of specimen measurements and instrumentation locations and Table 5 gives the values corresponding to the figure used for this specimen.

Table 6. GE02 bending instrumentation

Instrument Description	Local Instrument Name	Location	Channel No.
Strain gage, biaxial	SG5E_CA	On steel host pipe, crown, east side 5 in. from crack edge	Ch 0
Strain gage, biaxial	SG1E_CA	On steel host pipe, crown, east side 1 in. from crack edge	Ch 1
Strain gage, biaxial	SG1W_CA	On steel host pipe, crown, west side 1 in. from crack edge	Ch 2
Strain gage, biaxial	SG5W_CA	On steel host pipe, crown, west side 5 in. from crack edge	Ch. 3
Strain gage, biaxial	SG10E_IA	On steel host pipe, invert, east side 10 in. from crack edge	Ch. 4
Strain gage, biaxial	SG5E_IA	On steel host pipe, invert, east side 5 in. from crack edge	Ch. 5
Strain gage, biaxial	SG1E _IA	On steel host pipe, invert, east side 1 in. from crack edge	Ch. 6
Strain gage, biaxial	SG1W_IA	On steel host pipe, invert, west side 1 in. from crack edge	Ch. 7 .
Strain gage, biaxial	SG5W_IA	On steel host pipe, invert, west side 5 in. from crack edge	Ch. 8
Strain gage, biaxial	SG10W_IA	On steel host pipe, invert, west side 10 in. from crack edge	Ch. 9
Strain gage, biaxial	SG1E_CC	On steel host pipe, crown, east side 1 in. from crack edge	Ch. 10

Strain gage, biaxial	SG1W_CC	On steel host pipe, crown, west side 1 in. from crack edge	Ch 11
Strain gage, biaxial	SG5E_IC	On steel host pipe, invert, east side 5 in. from crack edge	Ch 12
Strain gage, biaxial	SG1E_IC	On steel host pipe, invert, east side 1 in. from crack edge	Ch. 13
Strain gage, biaxial	SG1W_IC	On steel host pipe, invert, west side 1 in. from crack edge	Ch. 14
Strain gage, biaxial	SG5W_IC	On steel host pipe, invert, west side 5 in. from crack edge	Ch.15
String potentiometer, 20 in. displacement	SP WW 28-20	On west saddle (centered), south springline, 20 in. from crack edge	SP0
String potentiometer, 10 in. displacement	SP W 24-10	On steel host pipe, west side, south springline, 2.5 in. from crack edge	SP1
String potentiometer, 10 in. displacement	SP E 29-10	On steel host pipe, east side, south springline, 2.5 in. from crack edge	SP2
String potentiometer, 3.8 in. displacement	SP EE 21-3	On east saddle (centered), south springline, 20 in. from crack edge	SP3
LVDT, AC	LVDT0 1001-EE	On backet on steel, west, invert, 1.5 in. from crack edge	LVDT Ch. 3
LVDT, AC	LVDT1 1002-E	On backet on steel, east, invert, 1.5 in. from crack edge	LVDT Ch. 1
LVDT, AC	LVDT2 1003-W	On bracket on steel, far west, invert, outside east load saddle, 23 in from crack edge	LVDT Ch. 2
LVDT, AC	LVDT 1004-WW	On bracket on steel, far east, invert, outside east load saddle, 23 in from crack edge	LVDT Ch. 0
LVDT SN1002, East, Invert, 23.5 in from crack edge	Applied Force	MTS Crosshead (Above Specimen)	
MTS Actuator Piston Position		MTS Crosshead (Above Specimen)	
150 psi Pressure Transducer	N/A	West endcap of specimen	Ch. 20

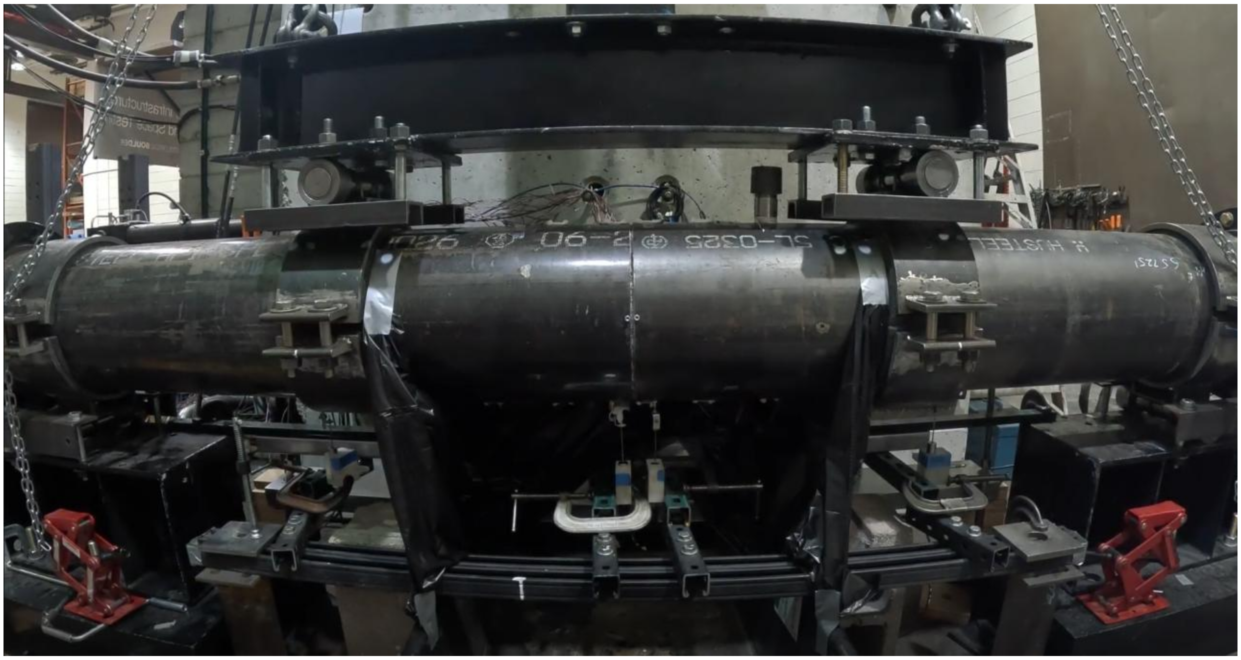

Figure 15. Photo of GE02 bending setup

Table 7. GE02 instrumentation schematic dimensions

Sensor / Measurement	Symbol	Distance
Strain Gauge (EE)	$L_{SG, EE}$	10 in
Strain Gauge (E)	$L_{SG, E}$	5 in
Strain Gauge (W)	$L_{SG, W}$	5 in
Strain Gauge (WW)	$L_{SG, WW}$	10 in
String Pot (EE)	$L_{SP, EE}$	19.75 in
String Pot (E)	$L_{SP, E}$	0.5 in
String Pot (W)	$L_{SP, W}$	2.5 in
String Pot (WW)	$L_{SP, WW}$	19.75 in
LVDT (EE)	$L_{L, EE}$	23 in
LVDT (E)	$L_{L, E}$	1.5 in
LVDT (W)	$L_{L, W}$	1.5 in
LVDT (WW)	$L_{L, WW}$	23 in
Distance between reaction and applied force	L_a	30 in
Distance between reactions	L_R	100 in
Distance between applied forces	L_m	40 in

4.1.3 GE_B01

The specimen for GE_B01 is composed of several steel host pipe segments joined together by two 22° flanged couplings and one 45° flanged coupling, shown in Figure 16. The specimen was rehabilitated with generic epoxy IRP and includes two initial gap openings of 0.5 in. (12.7 mm) located on either side of the 45° flanged coupling. Table 8 provides a detailed outline for instrumentation used for GE_B01, including instrument location, channel information, and instrument identifiers. The instrumentation consisted of strain gauges on the crown and invert over the middle 40 in. (1000 mm) (maximum moment) span, with some placed directly on the repair material, and others placed at areas of interest on the host pipe. LVDTs and SPs were vertically arranged to measure pipe deflection at various locations along the beam. These instruments were mounted on stands on the ground, with the opposite ends attached to the pipe using brackets or screw sockets. Four other LVDTs were set up on the crown and invert on each side of the 45° flanged coupling to measure changes across the initial gap openings. Figure 13 presents a visual diagram for instrumentation locations along the length of the pipe. Table 9 provides the values corresponding to the dimensions shown in Figure 13.

Table 8. GE_B01 bending instrumentation

Instrument Description	Local Instrument Name	Location	Channel No.
Strain gage, linear	HE20CA	Host Pipe, East, 20 in. from center, Crown, Axial	Ch 0
Strain gage, linear	HE20IA	Host Pipe, East, 20 in. from center, Invert, Axial	Ch 1
Strain gage, biaxial	RE09CA	Repair Material, East, 9 in. from center, Crown, Axial	Ch 2
Strain gage, biaxial	RE09CC	Repair Material, East, 9 in. from center, Crown, Circumferential	Ch. 3
Strain gage, biaxial	RE09IA	Repair Material, East, 9 in. from center, Invert, Axial	Ch. 4
Strain gage, biaxial	RE09IC	Repair Material, East, 9 in. from center, Invert, Circumferential	Ch. 5
Strain gage, linear	H00CA	Host Pipe, at center, Crown, Axial	Ch. 6
Strain gage, linear	H00IA	Host Pipe, at center, Invert, Axial	Ch. 7 .
Strain gage, biaxial	RW09CA	Repair Material, West, 9 in. from center, Crown, Axial	Ch. 8
Strain gage, biaxial	RW09CC	Repair Material, West, 9 in. from center, Crown, Circumferential	Ch. 9
Strain gage, biaxial	RW09IA	Repair Material, West, 9 in. from center, Invert, Axial	Ch. 10
Strain gage, biaxial	RW09IC	Repair Material, West, 9 in. from center, Invert, Circumferential	Ch 11
Strain gage, biaxial	HW20CA	Host Pipe, West, 20 in. from center, Crown, Axial	Ch 12

Strain gage, biaxial	HW20CC	Host Pipe, West, 20 in. from center, Crown, Circumferential	Ch. 13
Strain gage, linear	HW20IA	Host Pipe, West, 20 in. from center, Invert, Axial	Ch. 14
String potentiometer, 3.8 in. displacement	W25	West 25 in. from specimen center	SP0
String potentiometer, 3.8 in. displacement	C0	At center of specimen	SP1
String potentiometer, 10 in. displacement	E25	East 25 in. from specimen center	SP2
LVDT, AC	LVDT0 W25	West 25 in. from specimen center	LVDT Ch. 0
LVDT, AC	LVDT1 W10	West 10 in. from specimen center	LVDT Ch. 1
LVDT, AC	LVDT2 W6	West 6 in. from specimen center	LVDT Ch. 2
LVDT, AC	LVDT3 C0	At center of specimen	LVDT Ch. 3
LVDT, AC	LVDT4 E6	East 6 in. from specimen center	LVDT Ch. 4
LVDT, AC	LVDT5 E10	East 10 in. from specimen center	LVDT Ch. 5
LVDT, AC	LVDT6 E25	East 25 in. from specimen center	LVDT Ch. 6
LVDT, DC	LVDT7 PIW	Parallel to host pipe at location, Invert, West Gap	LVDT Ch. 7
LVDT, DC	LVDT8 PIE	Parallel to host pipe at location, Invert, East Gap	LVDT Ch. 8
LVDT, DC	LVDT9 PCW	Parallel to host pipe at location, Crown, West Gap	LVDT Ch. 9
LVDT, DC	LVDT10 PCE	Parallel to host pipe at location, Crown, East Gap	LVDT Ch. 10
LVDT SN1002, East, Invert, 23.5 in from crack edge	Applied Force	MTS Crosshead (Above Specimen)	
MTS Actuator Piston Position		MTS Crosshead (Above Specimen)	
150 psi Pressure Transducer	N/A	West end cap of specimen	Ch. 20

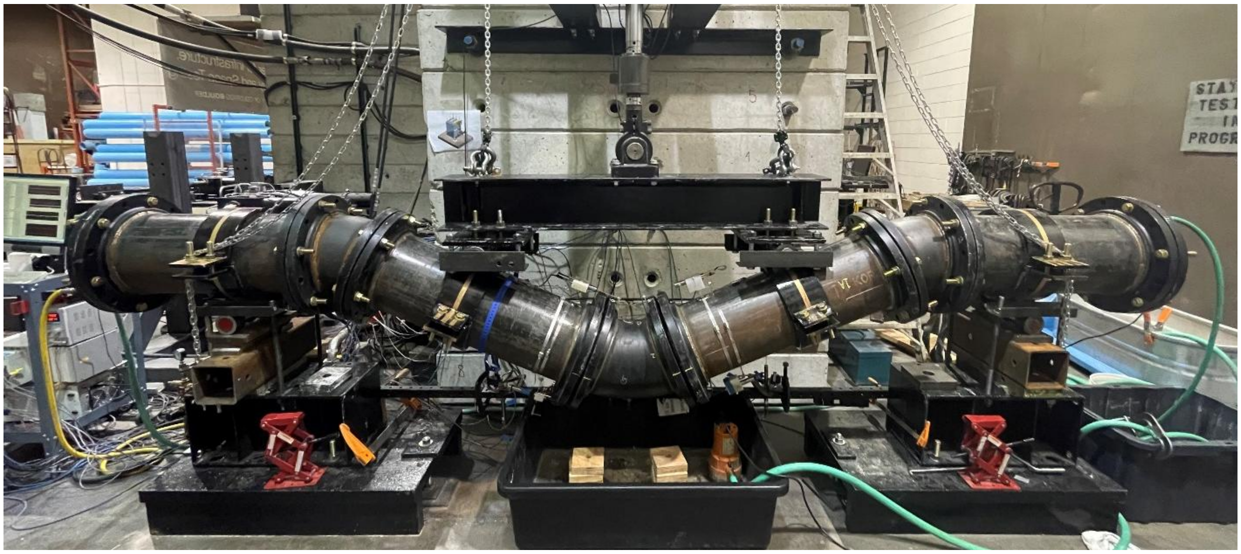

Figure 16. Photo of GE_B01 in bending setup

Table 9. GE_B01 instrumentation schematic dimensions

Sensor / Measurement	**Symbol**	**Distance**
Strain Gauge	L_{SG}	11 in
String Pot	L_{SP}	25 in
LVDT (6)	$L_{L,6}$	6 in
LVDT (10)	$L_{L,10}$	10 in
LVDT (25)	$L_{L,25}$	25 in
Distance between reaction and applied force	L_a	38.5 in
Distance between reactions	L_R	124 in
Distance between applied forces	L_m	47 in

4.1.4 GE_B02

The specimen for GE_B02 is composed of several steel host pipe segments joined together by two 22.5° flanged couplings and one 45° flanged coupling, shown in Figure 17. The specimen was rehabilitated with generic epoxy IRP and includes two initial gap openings of 0.5 in. (12.7 mm) located on either side of the 45° flanged coupling. Table 10 provides a detailed outline for instrumentation used for GE_B02, including instrument location, channel information, and instrument identifiers. The instrumentation consisted of strain gauges on the crown and invert over the middle 40 in. (1000 mm) (maximum moment) span, with some placed directly on the repair material, and others placed at areas of interest on the host pipe. Four strain gauges were added on the repair material on both sides to measure along the crack from crown to invert. LVDTs and SPs were vertically arranged to measure pipe deflection at various locations along the beam. These instruments were mounted on stands on the ground, with the opposite ends attached to the pipe using brackets or screw sockets. Two other LVDTs were set up on the crown to measure any movement of the saddles at the loading points. Figure 13 presents a visual diagram for instrumentation locations along the length of the pipe. Table 9 provides the values corresponding to the dimensions shown in Figure 13.

Table 10. GE_B02 bending instrumentation

Instrument Description	Local Instrument Name	Location	Channel No.
Strain gage, linear	HE20CA	Host Pipe, East, 20 in. from center, Crown, Axial	Ch 0
Strain gage, biaxial	H00CA	Repair Material, East, 9 in. from center, Crown, Axial	Ch 1
Strain gage, biaxial	RE09CC	Repair Material, East, 9 in. from center, Crown, Circumferential	Ch 2
Strain gage, linear	RW09CC	Repair Material, East, 9 in. from center, North shoulder, Axial	Ch. 3
Strain gage, linear	RE09CA	Repair Material, East, 9 in. from center, North haunch, Axial	Ch. 4
Strain gage, biaxial	RW09CA	Repair Material, East, 9 in from center, Invert, Axial	Ch. 5
Strain gage, biaxial	RW09IC	Repair Material, East, 9 in from center, Invert, Circumferential	Ch. 6
Strain gage, biaxial	NA	Repair Material, West, 9 in. from center, Crown, Axial	Ch. 7 .
Strain gage, biaxial	HE20IA	Repair Material, West, 9 in. from center, Crown, Circumferential	Ch. 8
Strain gage, linear	H00IA	Repair Material, West, 9 in. from center, North shoulder, Axial	Ch. 9
Strain gage, linear	NA	Repair Material, West, 9 in. from center, North haunch, Axial	Ch. 10
Strain gage, biaxial	RW09IA	Repair Material, West, 9 in from center, Invert, Axial	Ch 11
Strain gage, biaxial	NA	Repair Material, West, 9 in from center, Invert, Circumferential	Ch 12
Strain gage, biaxial	HW20CA	Host Pipe, West, 20 in. from center, Crown, Axial	Ch. 13
Strain gage, biaxial	HW20CC	Host Pipe, West, 20 in. from center, Crown, Circumferential	Ch. 14
String potentiometer, 3.8 in. displacement	W25	West 25 in. from specimen center	SP0

String potentiometer, 3.8 in. displacement	C0	At center of specimen	SP1
String potentiometer, 3.8 in. displacement	E25	East 25 in. from specimen center	SP2
LVDT, 3 in. stroke, AC	W26.5	West 26.5 in. from specimen center	LVDT Ch. 0
LVDT, 3 in. stroke, AC	C0	At center of specimen	LVDT Ch. 1
LVDT, 3 in. stroke, AC	W4	West 4 in. from specimen center	LVDT Ch. 2
LVDT, 3 in. stroke, AC	W14	West 14 in. from specimen center	LVDT Ch. 3
LVDT, 3 in. stroke, AC	E4	East 4 in. from specimen center	LVDT Ch. 4
LVDT, 3 in. stroke, AC	E14	East 14 in. from specimen center	LVDT Ch. 5
LVDT, 3 in. stroke, AC	E26.5	East 26.5 in. from specimen center	LVDT Ch. 6
LVDT, 3 in. stroke, DC	PCW	Parallel to host pipe at location, Crown, West saddle	DC Ch. 3
LVDT, 3 in. stroke, DC	PCE	Parallel to host pipe at location, Crown, East saddle	DC Ch. 2
	Applied Force	MTS Crosshead (Above Specimen)	
MTS Actuator Piston Position		MTS Crosshead (Above Specimen)	
150 psi Pressure Transducer	N/A	West end cap of specimen	Ch. 20

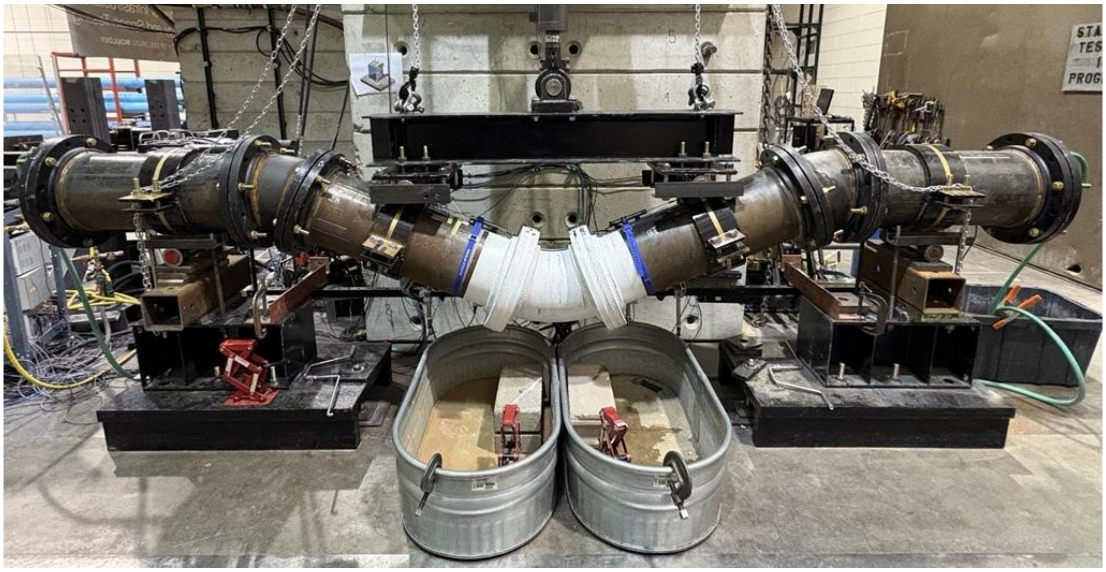

Figure 17. Photo of GE_B02 in bending setup

Table 11. GE_B02 instrumentation schematic dimensions

Sensor / Measurement	Symbol	Distance
Strain Gauge	L_{SG}	11.5 in
String Pot	L_{SP}	22 in
LVDT (6)	$L_{L,6}$	5 in
LVDT (10)	$L_{L,10}$	15 in
LVDT (25)	$L_{L,25}$	23.5 in
Distance between reaction and applied force	L_a	38.5 in
Distance between reactions	L_R	124 in
Distance between applied forces	L_m	47 in

4.2 Axial Testing

Axial testing follows the completion of transverse testing. Each specimen is oriented in a horizontal position supported by two supports with low friction Teflon pads between the specimen and the supports to reduce additional unwanted force measurements caused by friction. Specimens are tested with live pressure ranging from 0 psi to 65 psi, with most of the testing using the latter. For thermal cyclic testing, displacements are applied in the tensile direction at a quasi-static strain rate, then returned back to the actuator's initial displacement reading. Load is transferred to the specimens through the flanges with high strength threaded steel rods.

Target displacements are determined using methods described in Section 2.2. Relatively small initial displacements are applied to each specimen to establish an initial effective crack width, which provides initial target CODs for each specimen. The effective crack width is then recalculated after each set of thermal cycles, establishing a new target COD for subsequent cycles. For the first cycle of each set, an initial COD is measured due to pressurization of the specimen. This COD is included in the total COD for each set of tests (i.e., this displacement was considered to contribute to reaching the target crack opening displacement).

After 50 or more thermal cycles are applied to a specimen, ultimate capacity tests are performed. Ultimate capacity tests for each specimen generally include several loading and unloading instances, each with varying pressures or varying load rates. Details on these variations are discussed further in the results section (Section 5).

5 Test Results

The following sections provide the results for transverse loading for each specimen tested. Variations between test specimens are summarized in Section 4, Table 3.

5.1 GE01 Results

The specimen for GE01 is composed of a steel host pipe with nominal initial gap opening of 6 in. (152 mm) and rehabilitated with generic epoxy IRP. An overview of the operations performed on GE01 is provided in Table 12.

Table 12. Major mechanical procedures on GE01

General Operation	Num. of Cycles	Target Deformations
Traffic Cycles	500,000	0.044° Rotation
Small Adjacent Excavation	1	0.365° Rotation
Large Adjacent Excavation	1	0.707° Rotation

The specimen was first subjected to 500,000 traffic cycles at varying pressure levels, as outlined in Table 13. A sinusoidal displacement wave was applied transversely to achieve several different target rotations over the duration of testing. Tests were conducted at a frequency of 1 to 2 Hz throughout. Figure 18 illustrates the moment-rotation response for selected traffic cycles, representative of the overall performance across the testing duration.

Transverse displacements were applied to achieve rotations ranging from approximately 0.04° to 0.05°. The moment required to reach these rotations ranged from 7.0 kip-in. (0.8 kN-m) to 9.5 kip-in. (1.1 kN-m). The apparent stiffness was approximately 180 kip-in./deg. (20 kN-m/deg.) with no significant reduction in stiffness over time. The variations in the width of the cyclic loops are attributed to the rate of loading effects. Testing at 1 Hz resulted in narrow loops, while testing at 2 Hz resulted in wider responses.

Table 13. Testing details for GE01 traffic cycles

Test ID	Approx. Cycle	Internal Pressure [psi]	Loading Rate [Hz.]	Approx. Stiffness [kip-in./deg. (kN-m/deg.)]
BC02	1,000	10	1	173
BC03	44,000	10	1	165
BC05	100,000	10	2	176
BC08	200,000	30	2	165
BC11	300,000	30	2	191
BC13	400,000	65	2	176
BC15	500,000	65	2	180

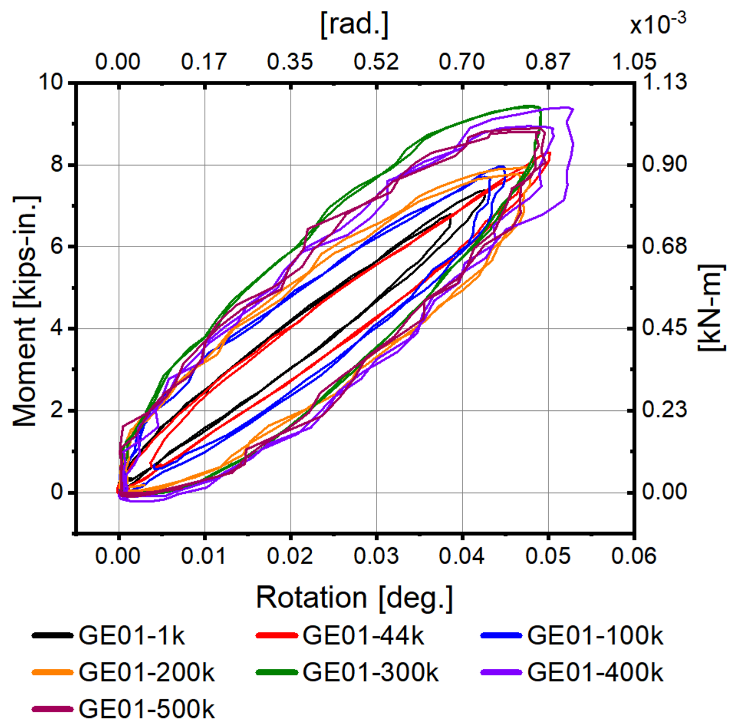

Figure 18. GE01 moment vs. rotation for selected traffic cycles

Following the application of 500,000 traffic cycles, two larger transverse deformations were applied to the specimen to simulate ground movement caused by adjacent excavation events. Figure 19 presents the actuator displacement and force over time for each lateral deformation applied. Additionally, this figure includes average measurements of the LVDTs positioned 1.5 in. (38 mm) on either side of the crack opening. Based on these measurements, the resultant rotation was calculated and plotted against the corresponding moment applied to the specimen, shown in Figure 20.

The first transverse displacement applied to the specimen simulated a smaller adjacent excavation (AE) event, while the second represented a larger, more significant excavation. During the first test, a maximum rotation of 0.45° was achieved at an applied moment of 54 kip-in. (6.1 kN-m), while the second test reached a maximum rotation of 0.65° at an applied moment of 75 kip-in. (8.5 kN-m) before system failure occurred (Figure 21-a),. The target rotation for the larger AE event was 0.707°. As rotation was applied, a rupture along the bottom side of the joint occurred, causing a complete loss in force capacity and internal pressure (Figure 21-b). The apparent stiffness for both AE events was approximately 120 kip-in./deg. (13.6 kN-m/deg.), which is 30% lower than the stiffness measured during traffic cycles (180 kip-in./deg.). Figure 21 shows test images prior to failure, at failure, and after failure.

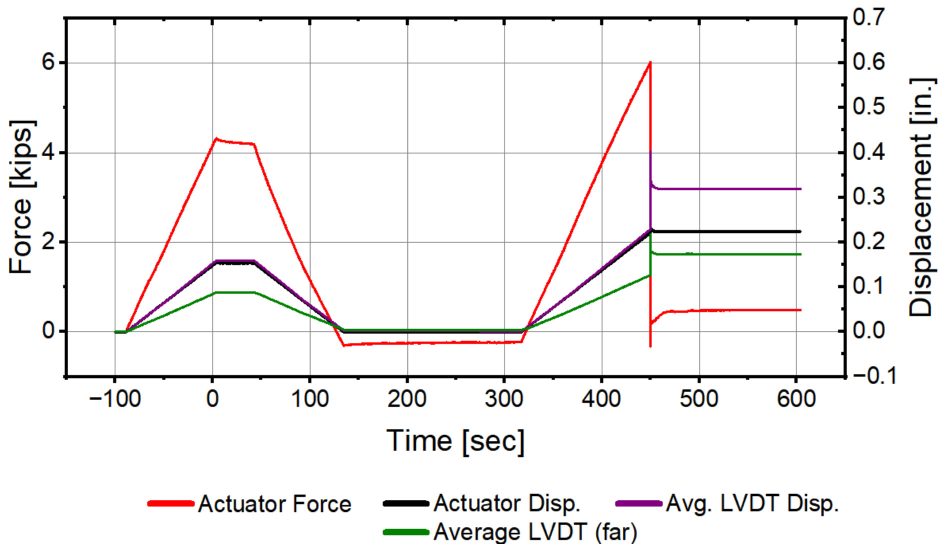

Figure 19. GE01 actuator displacement, actuator force, average LVDT displacement (center, purple) and Avg. LVDT Disp. (far, at the loading points, green) vs. time for adjacent excavation events

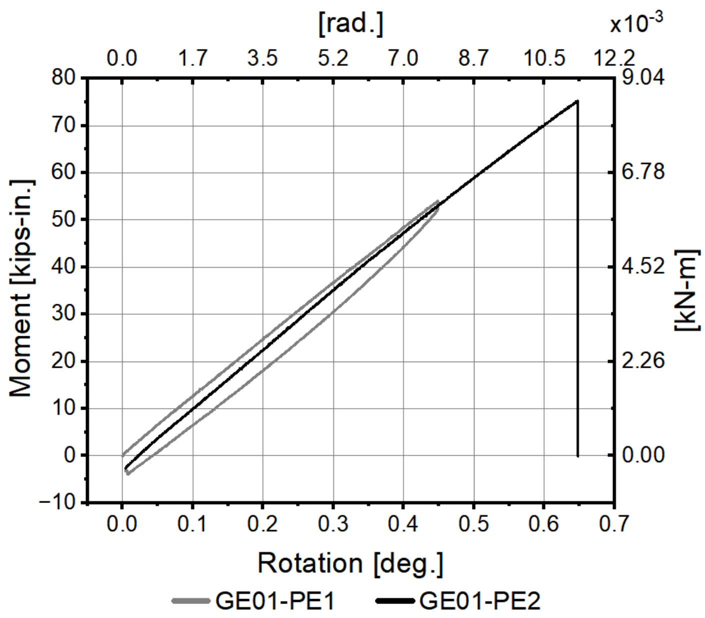

Figure 20. GE01 moment vs. rotation for adjacent excavation events

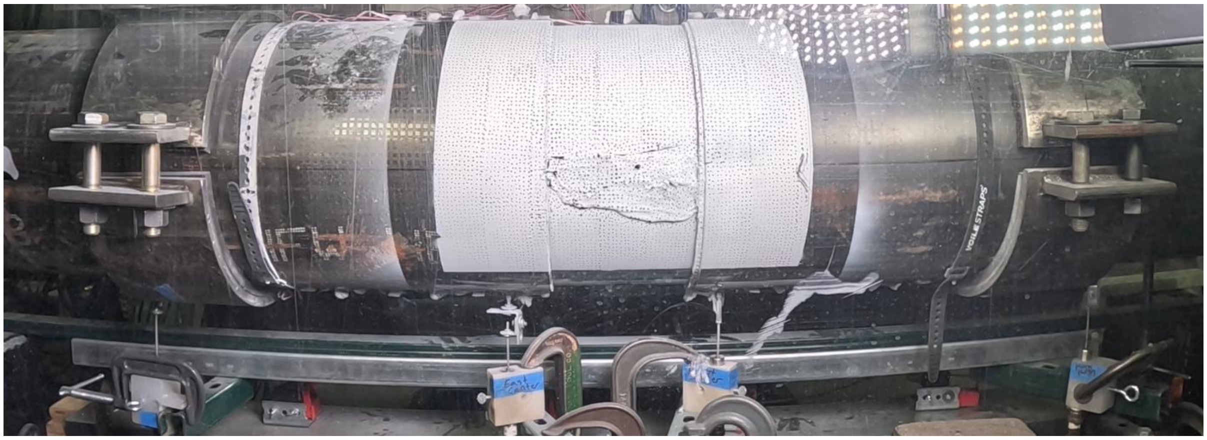

(a) Before failure

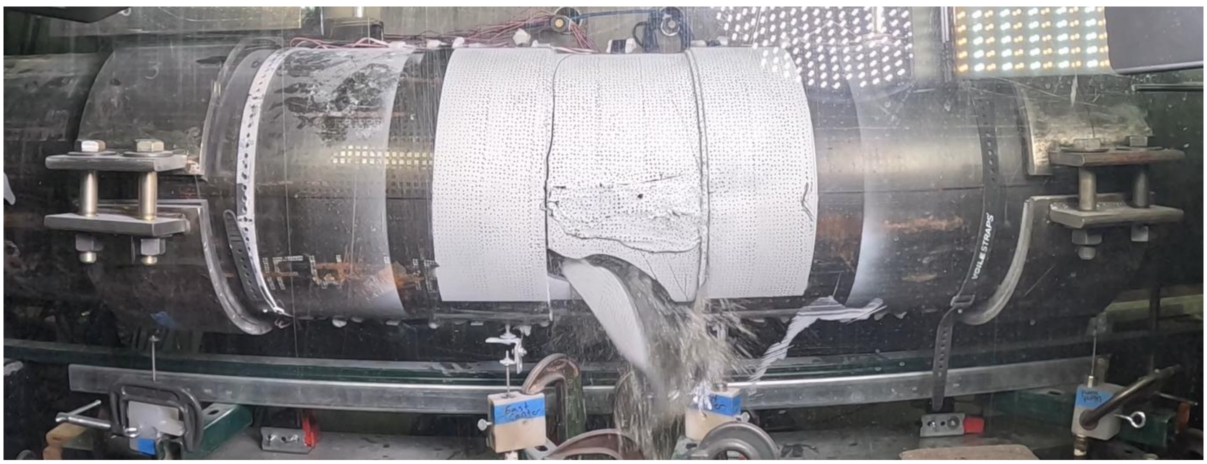

(b) At failure

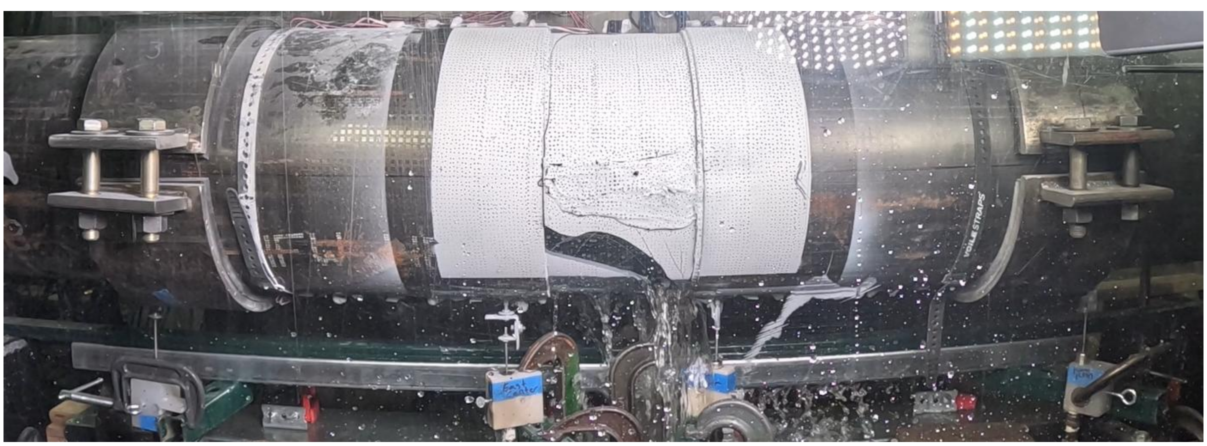

(c) After failure

Figure 21. GE01 testing sequence showing: (a) before failure, (b) at failure, and (c) after failure

5.2 GE02 Results

The specimen for GE02 is composed of a steel host pipe with an initial gap opening of 0.2 in. (5 mm) and rehabilitated with a generic epoxy IRP. An overview of the operations performed on GE02 is provided in Table 14.

Table 14. Major mechanical procedures on GE02

General Operation	Approx. Num. of Cycles	Target Displacement @ Crack edge (in.) [mm]	Target Rotation (degrees)	Test Pressure (psi)	Loading Rate [Hz.]
Traffic Cycles	0-25k	0.014 [0.36]	0.032°	10	1
	25k-45k	0.018 [0.46]	0.043°	10	1
	45k	0.025 [0.64]	0.06°	10	1

Testing began with the application of traffic cycles. A sinusoidal displacement was applied transversely to achieve a global target rotation of 0.081°. Tests were conducted at a frequency of 1 Hz throughout. During early stages of applied traffic loading, the specimen ruptured after about 45,000 cycles. Figure 22 illustrates the moment-rotation response for selected traffic cycles, representative of the overall performance across the testing duration. Rotations ranging from 0.03° to 0.06° were measured during selected traffic cycles. The moment required to reach these rotations ranged from 30 kip-in (3.4 kN-m) to 40 kip-in. (4.5 kN-m). In the initial cycles, the apparent stiffness was approximately 850 kip-in./deg. (96 kN-m/deg.). During the start of a cycle set intended to apply a rotation closer to the global target (0.081°), a sudden rupture occurred. The maximum rotation recorded was approximately 0.06° at a maximum applied moment of about 36 kip-in. (4.1 kN-m). Figure 23 shows the actuator force, actuator displacement, internal pressure, and average LVDT (close to center) measurements relative to time during failure. Further details about this test are presented in later sections of this report. No further testing was performed on this specimen.

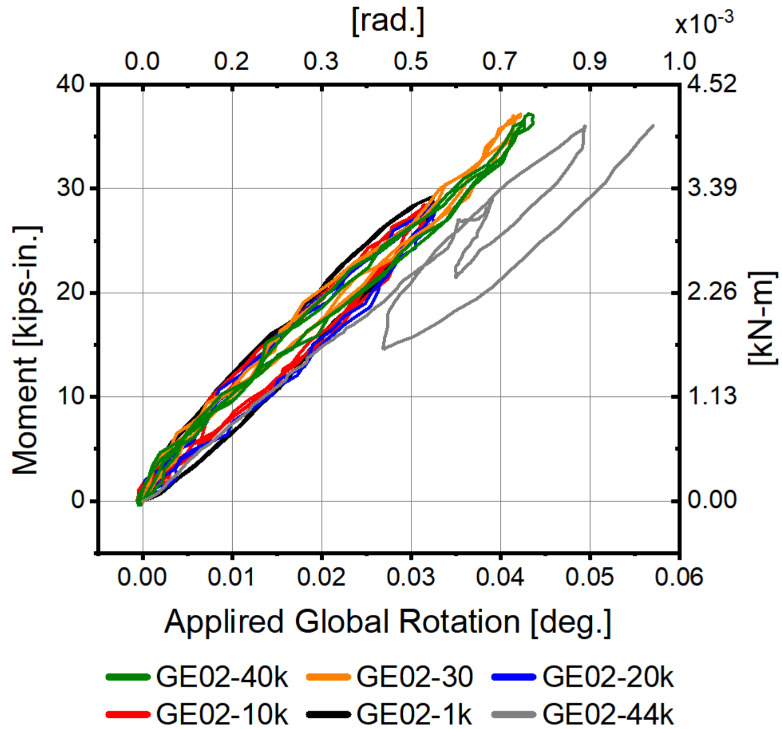

Figure 22. GE02 moment vs. rotation for selected traffic cycles

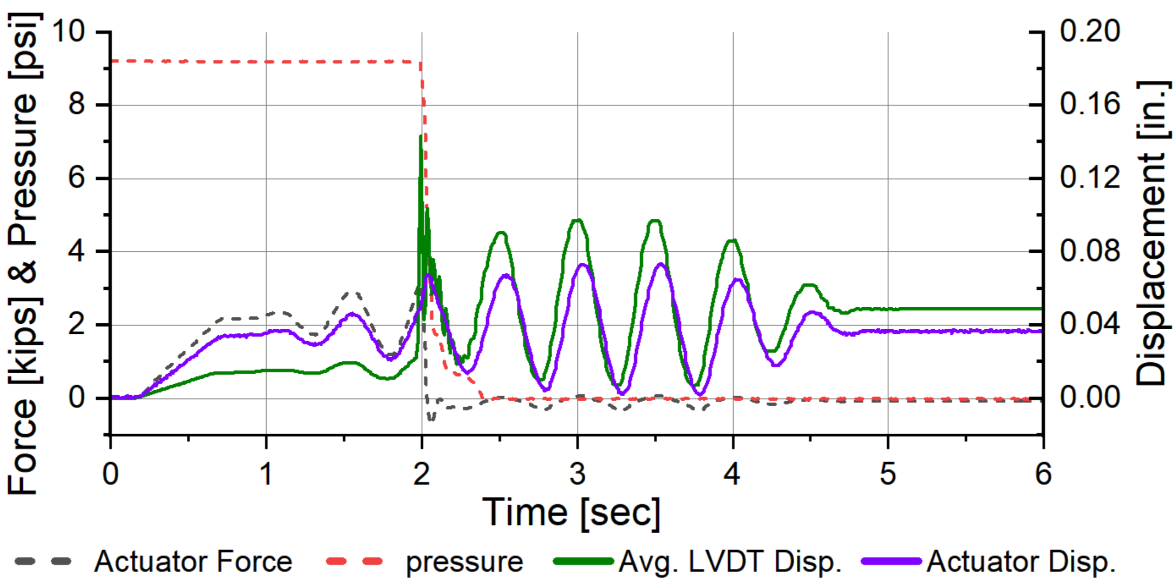

Figure 23. GE02 actuator displacement, actuator force, average LVDT displacement vs. time for bending cycle

5.3 GE_B01 Results

The specimen for GE_B01 is composed of several steel host pipe segments joined together by two 22° flanged couplings and one 45° flanged coupling. The specimen was rehabilitated with generic epoxy and includes two initial gap openings of 0.5 in. (12.7 mm) located on either side of the 45° flanged coupling. An overview of the operations performed on GE_B01 is provided in Table 15.

Table 15. Major mechanical procedures on GE_B01

General Operation	Num. of Cycles	Target Displacement @ Centerline (in.)	Target Rotation (degrees)	Test Pressure (psi)	Loading Rate (Hz)
Traffic Cycles	1-15k	0.015	0.036°	10	1
	15k-79k	0.033	0.061°	10	1
	79k-100k	0.033	0.061°	10	2
	100k-348k	0.033	0.061°	30	2
	348k-500k	0.033	0.061°	65	2
Adjacent Excavation	1	0.26	0.506°	65	0.083

The specimen was subjected to 500,000 traffic cycles. As noted in Table 15, the internal pressure and loading rate increased as testing progressed. A sinusoidal displacement wave was applied transversely to achieve target rotations ranging from 0.036° to 0.061°. The moment required to reach these rotations ranged from 25 kip-in. (2.8 kN-m) to 36 kip-in. (4.0 kN-m). The apparent stiffness was approximately 460 kip-in./deg. (53 kN-m/deg.). Figure 24 illustrates the moment-rotation response for selected traffic cycles, representative of the overall performance across the testing duration.

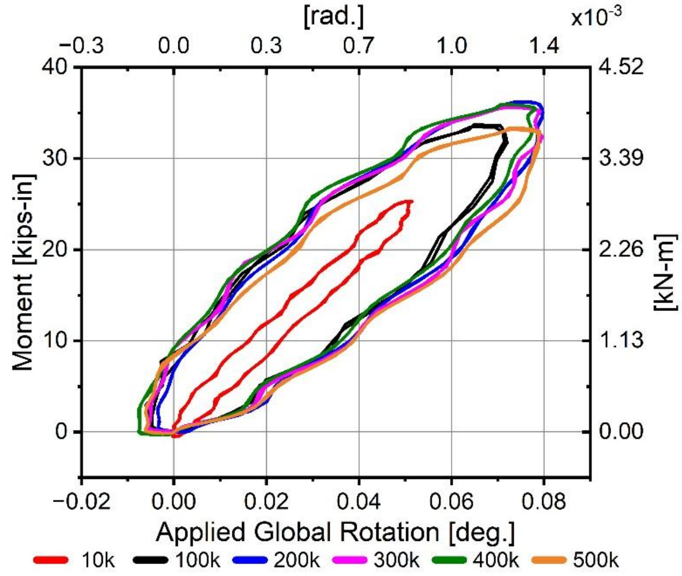

Figure 24. GE-B01 moment vs. rotation for selected traffic cycles

Following the application of 500,000 traffic cycles, larger transverse deformations were applied to the specimen to simulate ground movement caused by adjacent excavation events. Two lateral pushes were planned with target displacements of 0.26 in. and 0.52 in. to simulate smaller and larger AE events, respectively, however system failure occurred during the first push. Figure 25 presents the actuator displacement and force over time for the lateral deformation applied. Based on these measurements, the resultant rotation was calculated and plotted against the corresponding moment applied to the specimen, shown in Figure 26.

The target rotation for the first adjacent excavation event was 0.506°. After a rotation of 0.286° was applied, a rupture occurred at the west gap and the liner cracked around the entire circumference, splitting the specimen in two. The force applied to the specimen reached a maximum of 4.8 kips before the rupture occurred. The apparent stiffness of the specimen before failure was approximately 210 kip-in./deg, which is over 50% lower than the stiffness measured during traffic cycles (460 kip-in./deg). Figure 27 shows images of the specimen at failure, the crack as observed from the crown of the pipe, and the crack as observed from the north springline of the pipe.

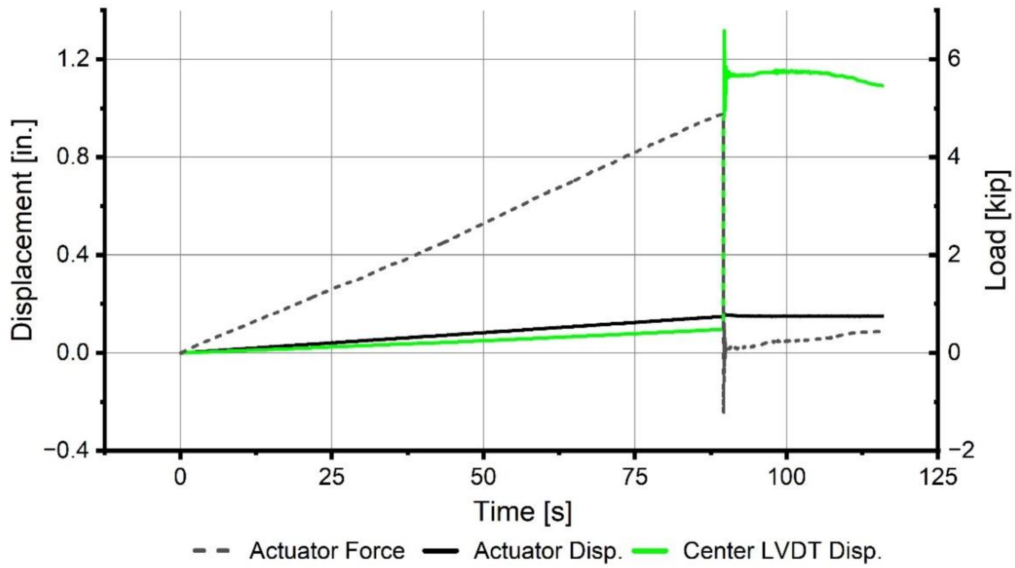

Figure 25. GE_B01 actuator displacement, actuator force, center LVDT displacement vs. time for adjacent excavation event

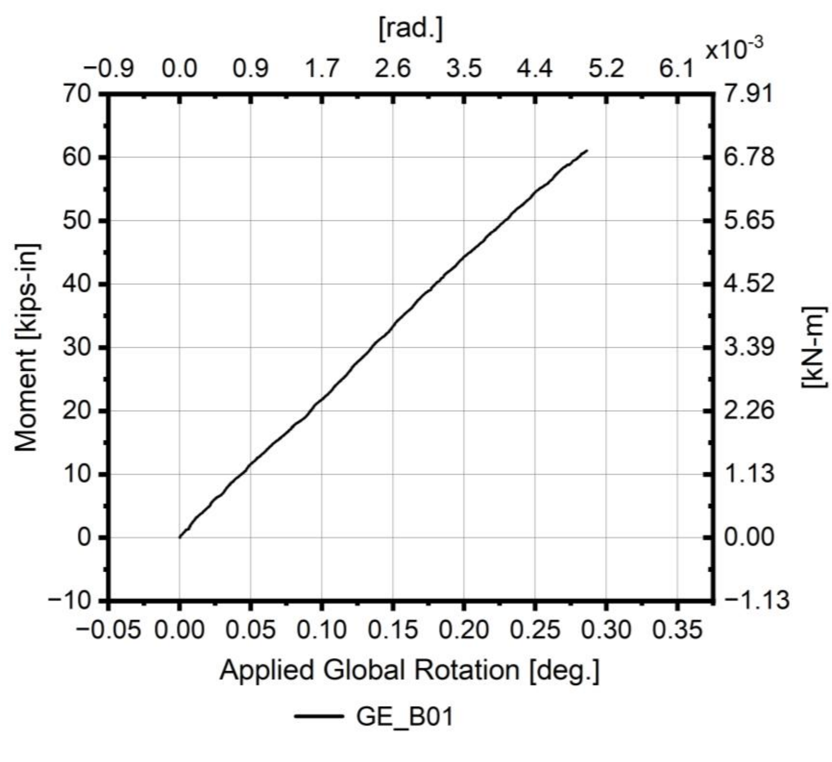

Figure 26. GE_B01 moment vs applied global rotation for adjacent excavation event

(a) (b) (c)

Figure 27. GE_B01 adjacent excavation photos, showing (a) moment of failure, (b) west crack from pipe crown and (c) west crack from north springline

After the ultimate capacity was reached, the specimen was removed from the frame so the cross-section at the failed crack could be examined. The IRP thickness was measured at multiple points along the cross-section as there was some variation. Table 16 lists the measured thicknesses at the pipe crown, springlines and invert. Figure 28 shows photos of the cross-section at the west gap, where variation in thickness can be seen.

Table 16. GE_B01 IRP thickness at failed west gap

Location	Average Thickness (in. [mm])
Crown	0.417 [10.6]
North Shoulder	0.382 [9.7]
North Springline	0.326 [8.3]
North Haunch	0.814 [20.7]
Invert	0.730 [18.5]
South Haunch	0.807 [20.5]
South Springline	0.303 [7.7]
South Shoulder	0.312 [7.9]
Average Thickness (in. [mm])	0.512 [13.0]

(a) (b)

Figure 28. Photos of GE_B01's cross-section at failed west gap, (a) shows east side and (b) shows west side

5.4 GE_B02 Results

The specimen for GE_B02 is composed of several steel host pipe segments joined together by two 22° flanged couplings and one 45° flanged coupling. The specimen was rehabilitated with generic epoxy IRP and includes two initial gap openings of 0.5 in. (12.7 mm) located on either side of the 45° flanged coupling. An overview of the operations performed on GE_B02 is provided in Table 17.

Table 17. Major mechanical procedures on GE_B02

General Operation	Num. of Cycles	Target Displacement @ Centerline (in.)	Target Rotation (degrees)	Test Pressure (psi)	Loading Rate (Hz)
Traffic Cycles	1-7k	0.015	0.028°	10	1
	7k-17k	0.02	0.038°	10	1
	17k-37k	0.031	0.057°	10	1
	37k-112k	0.031	0.057°	10	2
	112k-306k	0.031	0.057°	30	2
	306k-355k	0.031	0.057°	45	2

	355k-378k	0.031	0.057°	65	2

The specimen has been subjected to 378,576 out of 500,000 traffic cycles. As noted in Table 17, the internal pressure and loading rate increased as testing progressed. After approximately 64,000 cycles, a slow leak around 1 drop every 10 seconds was noticed, and the leakage rate increased as testing progressed. The specimen was unable to hold any internal pressure after approximately 378,400 cycles which corresponded to a fracture in the IRP. A sinusoidal displacement wave was applied transversely to achieve target rotations ranging from 0.028° to 0.057°. The moment required to reach these rotations ranged from 15 kip-in. (1.7 kN-m) to 30 kip-in. (3.4 kN-m). The apparent stiffness was approximately 390 kip-in./deg. (44 kN-m/deg.). Figure 29 illustrates the moment-rotation response for selected traffic cycles, representative of the overall performance across the testing duration. Figure 30 shows a photo of the fracture that occurred at the west haunch/invert of the liner.

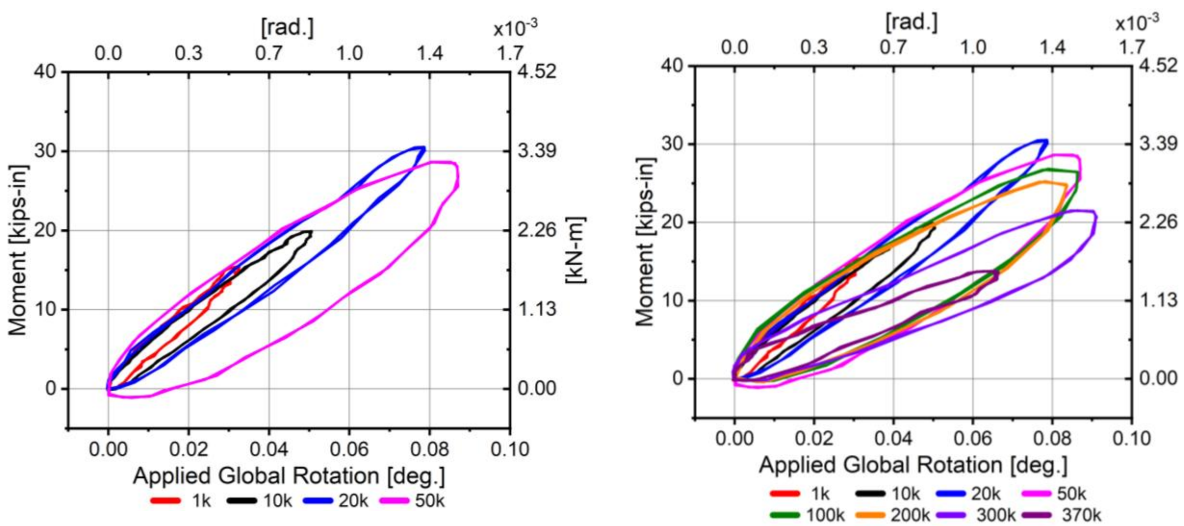

(a) **(b)**

Figure 29. GE_B02 moment vs. applied global rotation for selected traffic cycles (a) before first leak and (b) for remaining applied cycles

Figure 30. GE_B02 photo of fracture after 378,400 cycles, located at the west invert / south haunch of the liner

After the ultimate capacity was reached, the specimen was removed from the frame so the cross-section at the failed crack could be examined. The IRP thickness was measured at multiple locations along the cross-section as there was some variation. Table 18 lists the measured thicknesses at the pipe crown, springlines and invert. The liner was very thin at the crown and south shoulder, so IRP thickness was not measured at those locations. Figure 31 shows photos of the cross-section at the west gap, where variation in thickness can be seen. Figure 32 shows the liner thickness specifically at the crown, where liner thickness was not measured.

Table 18. GE_B02 IRP thickness at failed west gap

Location	Average Thickness (in. [mm])
Crown	---
North Shoulder	0.110 [2.8]
North Springline	0.367 [9.3]
North Haunch	0.647 [16.4]
Invert	1.226 [31.1]
South Haunch	0.607 [15.4]
South Springline	0.330 [8.4]
South Shoulder	---
Average Thickness including thin sections as 0 in. thick (in. [mm])	0.411 [10.4]

Average Thickness excluding thin sections (in. [mm])	0.548 [13.9]

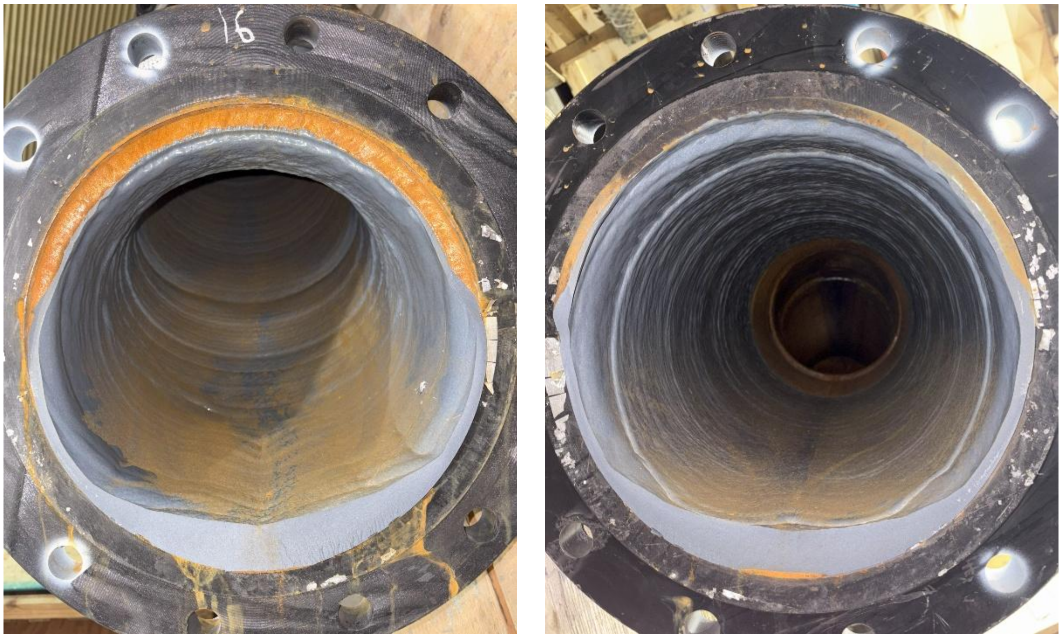

(a) (b)

Figure 31. Photos of GE_B02's cross-section at failed west gap, (a) shows east side and (b) shows west side

(a) (b)

Figure 32. Photos of GE_B02's liner thickness at crown, (a) east side and (b) west side of failed gap

6 Discussion of Results

Four specimens composed of a steel host pipe with nominal initial gap openings of 6.0 in. (GE01), 0.25 in. (GE02), cumulative gap openings of 1.0 in. (GE_B01 and GE_B02) and rehabilitated with generic epoxy IRP were tested. Each specimen started the same testing program, which includes the application of 600,000 traffic cycles, 2 larger adjacent excavation (AE) events, 50 thermal expansion cycles, and a final ultimate axial capacity test. GE01 reached ultimate capacity during the second AE event, and GE02 reached capacity after 44,700 traffic cycles. GE_B01 reached ultimate capacity during the first AE event. GE_B02 reached ultimate capacity after 378,400 traffic cycles, presumably failing earlier in testing due to the liner application rather than the material of the liner itself.

Figure 33 shows the moment relative to rotation during the instance of failure for GE01, GE02, GE_B01 and GE_B02. The maximum applied moment for GE01 was around 75 kip-in. (8.5 kN-m) at a maximum rotation of about 0.65°. The maximum applied moment for GE02 was around 36 kip-in. (4.1 kN-m) at a maximum rotation of about 0.6°. The maximum applied moment for GE_B01 was around 61 kip-in. (6.9 kN-m) at a maximum rotation of about 0.28°. Each specimen exhibited predominantly linear behavior, with a sudden material fracture and limited apparent softening phase.

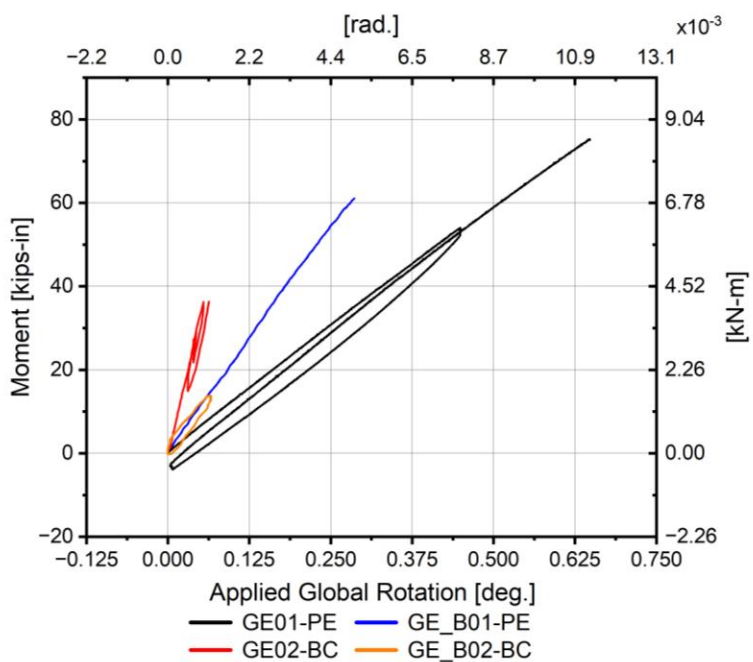

Figure 33. Moment vs. rotation at instances of ultimate capacity for GE01, GE02, GE_B01 and GE_B02

During the early phase of testing, the moment-ration behaviors of GE01, GE02, GE_B01 and GE_B02 were examined, as shown in Figure 34. Among these specimens, GE01 exhibited the largest gap opening and thus underwent the highest deformation demands under cyclic loading. By contrast, GE02, which featured a smaller gap opening, demonstrated the greatest stiffness at 893 kip-in./deg. (100.9 kN-m/deg.). Meanwhile, GE_B01, incorporating two gap openings at different positions, showed an intermediate stiffness of 516 kip-in./deg. (58.3 kN-m/deg.). GE_B02, also exhibited an intermediate stiffness of 475 kip-in./deg. (53.7 kN-m/deg.), slightly less than GE_B01 which had the same geometry and gap size. It is noteworthy that GE01 displayed the lowest measured stiffness of 186 kip-in./deg. (21.0 kN-m/deg.), further highlighting the correlation between gap size and stiffness. Despite these variations in behavior, GE02 and GE_B01 experienced similar levels of applied global rotation during the early cycles, underscoring the potential impact of local gap configurations on the overall deformation response. More testing is required to further understand how specimen geometry changes the response under consistent testing methods.

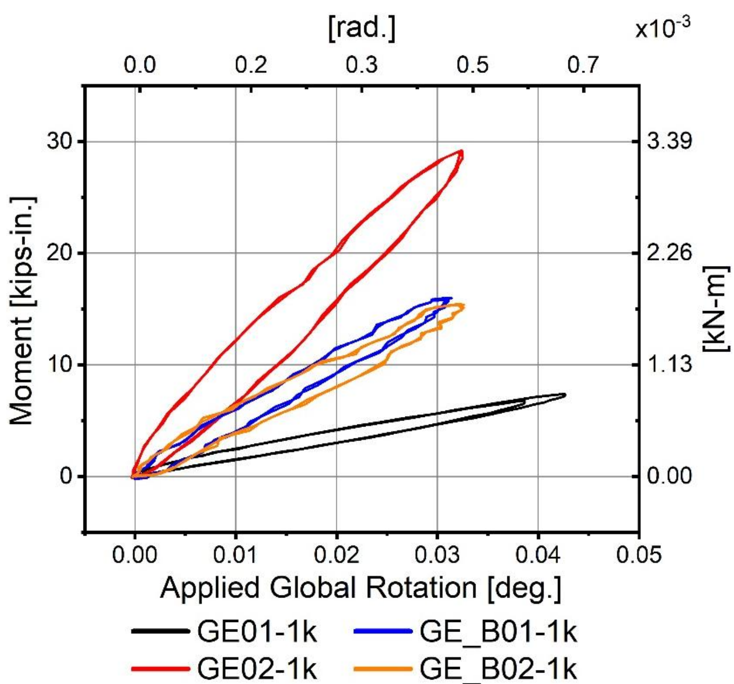

Figure 34: Moment vs. rotation at Early cycles for GE01, GE02, GE_B01 and GE_B02

7 Summary & Conclusions

This section summarizes the findings of the testing program performed on 12 in. (300-mm) diameter specimens repaired with a generic epoxy material. Straight steel host pipe specimens were prepared and tested with nominal 6 in. (150 mm) or 0.5 in. (12.7 mm) gaps of exposed epoxy IRP, with approximately 5 ft (1.52 m) of host pipe on either side of the gap. Two additional, first-of-their-kind bent pipe specimens were also tested, each with two 0.5 in. (150mm) exposed sections of IRP on either side of a 45-degree elbow. They were subjected to cyclic flexural loading using specialized testing equipment at the Center for Infrastructure, Energy, and Space Testing (CIEST) at the University of Colorado Boulder.

The general methodology consisted of applying transverse deformation to a pipe specimen. Target bending involved 500,000 short duration (1 to 2 Hz) cycles representing cyclic deformation caused by overhead traffic. This fatigue testing was followed by larger bending deformations reflective of the system responses to adjacent excavation activity.

The levels of excavation movement assumed for the adjacent excavation cycles were associated with 2.5 in. (63.5 mm) and 5 in. (127 mm) for the small and large events, respectively. The 5 in. (127 mm) level of soil displacement is expected to be used to set maximum parallel excavation deformation levels in future studies and testing standards. The targeted rotational deformations depend on the stiffness of the repair pipe and the nature of the bonding between the repair and host pipe. If another IRP technology had a similar stiffness to the generic epoxy system, similar deformation levels would be anticipated. Initial stiffness tests of specimens and comparison with analytical and/or numerical models will inform the degree of bonding and, thus, deformation levels (for example see Klingaman et al., 2024).

The stiffness of the specimens in bending ranged from roughly 180 to 850 kip-in./deg (20 - 96 kN-m/deg), using a global rotation calculated by LVDTs positioned on either side of the crack opening, or at the center of the specimen. The initial crack width and specimen geometry influenced differences in stiffness among specimens. Maximum moments achieved in the lateral loading of straight specimens ranged from 9.5 kip-in. to 40 kip-in. (1.1 kN-m to 4.5 kN-m), and maximum moments of the bent specimens ranged from 30 kip-in. to 36 kip-in. (3.4 kN-m to 4.0 kN-m).

While all generic epoxy repair system specimens did not complete all testing sequences outlined herein, most specimens performed well under cyclic transverse loading. Underperformance of specimens corresponded to localized reduction of IRP material thickness at irregular deviations in host pipe internal diameter (i.e., at locations of host pipe gap). While fracture of the specimen occurred at these locations before completing the entire testing sequences, these thickness changes can be adequately addressed through further application development (e.g., application of multiple IRP layers at locations of irregular host pipe inner geometry). The testing program demonstrated that the IRP system has significant promise as a trenchless pipeline repair system for both straight pipe sections and those with bends typical of in-service systems and, with relatively minor alterations to the technology, has the potential to successfully meet the performance expectations of this rigorous 50-year mechanical aging assessment program.

References

Ahmadi, H., Manalo, A., Dixon, P.G., Salah, A., Karunasena, W., Tien, C.M.T., … Wham, B.P. (2024). "Temperature change-induced linear and nonlinear axial responses of internal replacement pipe (IRP) systems for pipeline rehabilitation incorporating the effects of soil friction". *Structures*, *62*(March), 106247. doi.org/10.1016/j.istruc.2024.106247

Allouche, E.N., Alam, S., Simicevic, J., Sterling, R., Condit, W., Matthews, J., & Selvakumar, A. (2014). "A pilot study for retrospective evaluation of cured-in-place pipe (CIPP) rehabilitation of municipal gravity sewers". *Tunnelling and Underground Space Technology*, *39*, 82–93. doi.org/10.1016/j.tust.2012.02.002

ASME. (2018). *Article 403 Nonmetallic Internal Line for Pipe: Sprayed Form for Buried Pipe*. *ASME PCC-2-2018 Repair of Pressure Equipment and Piping*. New York: ASME.

ASTM. (2016a). "F3182 - 16 Standard practice for the application of spray-applied polymeric liners inside pipelines for potable water". *ASTM International*. West Conshohocken, PA. doi.org/10.1520/F3182

ASTM. (2016b, August 1). "F1216: Practice for Rehabilitation of Existing Pipelines and Conduits by the Inversion and Curing of a Resin-Impregnated Tube". West Conshohocken, PA: ASTM International. doi.org/10.1520/F1216-16

ASTM. (2017, February). "F1743: Practice for Rehabilitation of Existing Pipelines and Conduits by Pulled-in-Place Installation of Cured-in-Place Thermosetting Resin Pipe (CIPP)". West Conshohocken, PA: ASTM International. doi.org/10.1520/F1743-17

ASTM. (2018). "D5813 - 04 Standard Specification for Cured-In-Place Thermosetting Resin Sewer Piping Systems". doi.org/10.1520/D5813-04R18

ASTM. (2019). "F2207-06: Standard Specification for Cured-in-Place Pipe Lining System for Rehabilitation of Metallic Gas Pipe". West Conshohocken, PA. doi.org/10.1520/F2207-06R19

AWWA. (2019). "Committee Report: Structural Classifications of Pressure Pipe Linings". American Water Works Association (AWWA).

Dixon, P.G., Salah, A., Ahmadi, H., Ulrich, M.E., Hubler, M.H., Dashti, S., … Wham, B.P. (2023a). "An Analytical Approach for Thermally Induced Axial Deformation in Rehabilitated Pipelines". *Proceedings: Pipelines 2023* (pp. 260–269). Reston, VA: American Society of Civil Engineers. doi.org/10.1061/9780784485026.028

Dixon, P.G., Tafsirojjaman, T., Klingaman, J., Hubler, M.H., Dashti, S., O'Rourke, T.D., … Wham, B.P. (2023b). "State-of-the-Art Review of Performance Objectives for Legacy Gas Pipelines with Pipe-in-Pipe Rehabilitation Technologies". *Journal of Pipeline Systems Engineering and Practice*, *14*(2), 1–13. doi.org/10.1061/JPSEA2.PSENG-1371

Fu, G., Shannon, B., Rathnayaka, S., Deo, R., & Kodikara, J. (2020). *State of The Art Literature Review on CIPP liners*. *CRC Project: Smart Linings for Pipe and Infrastructure*.

Jeon, S.-S., O'Rourke, T.D., Neravali, A.N., O'Rourke, T.D., & Neravali, A.N. (2004). "Repetitive Loading Effects on Cast Iron Pipelines with Cast-in-Place Pipe Lining Systems". *Journal of Transportation Engineering*, *130*(6), 692–705. doi.org/10.1061/(ASCE)0733-947X(2004)130:6(692)

Klingaman, J., Dixon, P.G., Wham, B.P., Dashti, S., & Hubler, M.H. (2022). "Traffic Loading Effects on

Rehabilitated Cast Iron Distribution Pipelines". *Proceedings: Pipelines 2022* (pp. 313–323). Reston, VA: American Society of Civil Engineers. doi.org/10.1061/9780784484296.037

Klingaman, J., Wham, B.P., Dixon, P.G., & Dashti, S. (2025). "External loading-induced deformations of deteriorated pipelines rehabilitated with internal replacement technologies". *Tunnelling and Underground Space Technology*, *157*(March), 106272. doi.org/10.1016/j.tust.2024.106272

Lu, H., Behbahani, S., Azimi, M., Matthews, J.C., Han, S., & Iseley, T. (2020). "Trenchless Construction Technologies for Oil and Gas Pipelines: State-of-the-Art Review". *Journal of Construction Engineering and Management*, *146*(6), 03120001. doi.org/10.1061/(asce)co.1943-7862.0001819

Najafi, M. (2005). *Trenchless Technology: Pipeline and Utility Design, Construction, and Renewal (Design considerations for trenchless renewal methods)* (1st ed.). New York: McGraw-Hill Education. Retrieved from https://www.accessengineeringlibrary.com/content/book/9780071422666

Roboski, J., & Finno, R.J. (2006). "Distributions of ground movements parallel to deep excavations in clay". *Canadian Geotechnical Journal*, *43*(1), 43–58. doi.org/10.1139/t05-091

Stewart, H.E., O'Rourke, T.D., Wham, B.P., Netravali, A.N., Argyrou, C., Zeng, X., & Bond, T.K. (2015). "Performance Testing of Field-Aged Cured-in-Place Liners (CIPL) for Cast Iron Piping". Cornell University, Ithaca, NY.

Vladeanu, G., & Matthews, J.C. (2018). "Analysis of risk management methods used in trenchless renewal decision making". *Tunnelling and Underground Space Technology*, *72*(November 2017), 272–280. doi.org/10.1016/j.tust.2017.11.025